CHAPTER

14

Aerodynamics

OUTLINE

CHAPTER OBJECTIVES

- To introduce the fundamental concepts and vocabulary associated with aircraft and aerodynamics
- To quantify the ideal-flow performance of simple two-dimensional airfoil sections
- To present the lifting line theory of Prandtl and Lanchester for a finite-span wing
- To describe the means by which fish, birds, insects, and sails exploit lift forces for flight and/or propulsion

14.1. INTRODUCTION

Aerodynamics is the branch of fluid mechanics that deals with the determination of the fluid mechanical forces and moments on bodies of interest. The subject is called *incompressible aerodynamics* if the flow speeds are low enough (Mach number < 0.3) for compressibility effects to be negligible. At larger Mach numbers where fluid-compressibility effects are important the subject is normally called *gas dynamics*. Aerodynamic parametric ranges of interest are usually consistent with: 1) neglecting buoyancy forces and fluid stratification, 2) assuming uniform constant-density flow upstream of the body, and 3) presuming viscous effects are confined to thin boundary layers adjacent to the body surface (Figure 9.1). Airfoil stall is a notable exception to this last presumption.

This chapter presents the elementary aspects of incompressible aerodynamics of aircraft wing shapes. Thus, with the simplifications just stated, the flows considered here are primarily ideal flows, and a significant portion of the material in Chapter 6 is relevant here. In addition, much of the material in this chapter also applies to ship propellers and to turbomachines (e.g., fans, turbines, compressors, and pumps) since the blades of these devices may all have similar cross sections.

14.2. AIRCRAFT TERMINOLOGY

Modern commercial aircraft embody nearly all the principles of aerodynamics presented in this chapter. Thus, a review of aircraft terminology and control strategies is provided in this section. Figure 14.1 shows three views of a commercial airliner. The body of the aircraft, which houses the passengers and other payload, is called the *fuselage*. The engines (jet or propeller) are often attached to the wings but they may be mounted on the fuselage too. Figure 14.2 shows an overhead (or planform) view of an airliner wing. The location where a wing attaches to the fuselage is called the *wing root*. The outer end of a wing furthest from the fuselage is called the *wing tip*, and the distance between the wing tips is called the *wingspan*, s. The distance between the leading and trailing edges of the wing is called the *chord length*, c, and it varies in the span-wise direction. The area of the wing when viewed from above is called the *planform area*, A. The slenderness of the wing planform is measured by its *aspect ratio*:

$$\Lambda \equiv s^2/A = s/\bar{c}, \quad \text{where } \bar{c} = A/s \tag{14.1, 14.2}$$

is the average chord length.

The various possible rotational motions of an aircraft can be referred to three aircraft-fixed axes, called the *pitch axis*, the *roll axis*, and the *yaw axis* (Figure 14.3). A positive aerodynamic drag force points opposite to the direction of flight. Negative drag is called *thrust* and it must be produced by the aircraft's engines for full execution of the aircraft's flight envelope (take-off, cruise, landing, etc.). Lift is the aerodynamic force that points perpendicular to the direction of flight. It must be generated by the wings to counter the weight of the aircraft in flight. Movable surfaces on the wings and tail fin, known as *control surfaces*,

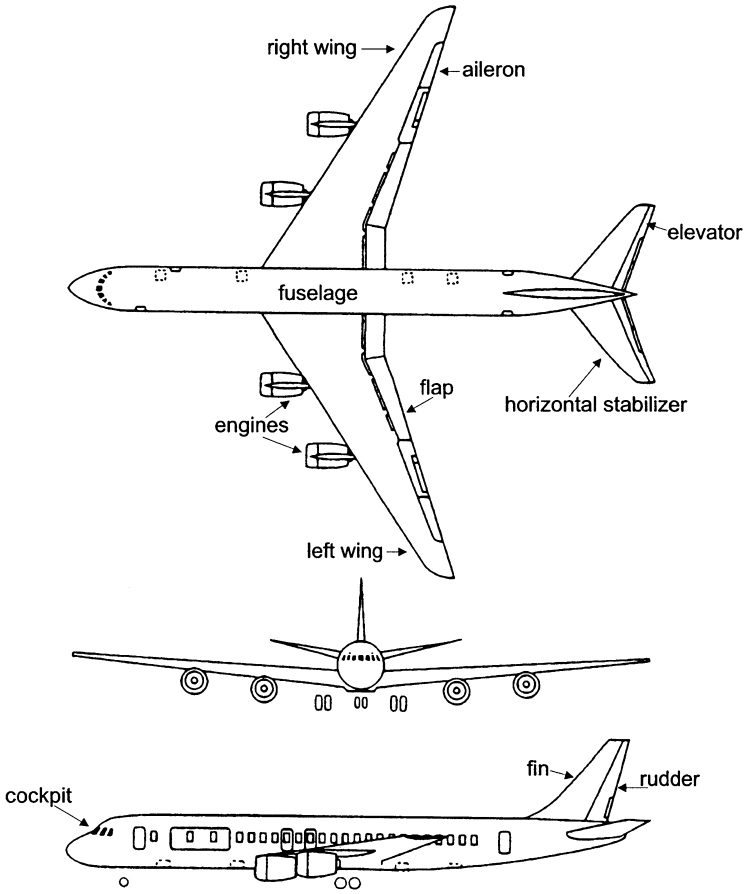

FIGURE 14.1 Three views of a commercial airliner and its control surfaces (NASA). The top view shows the wing planform. The wing is both backward swept and tapered. The various control surfaces shown modify the trailing edge geometry of the wing and tail fins. Landing gear details have been omitted.

can alter the distribution of lift and drag forces on the aircraft and provide the primary means for controlling the direction of flight. However, variation of engine thrust can also be used to steer the aircraft.

Control Surfaces

The aircraft is controlled by the pilot seated in the *cockpit*, who—with hydraulic assistance—sets the engine thrust and moves the control surfaces described in the following paragraphs. For the most part, these control surfaces act to change the local *camber* or curvature of the wings or fins to alter the lift force generated in the vicinity of the control surface.

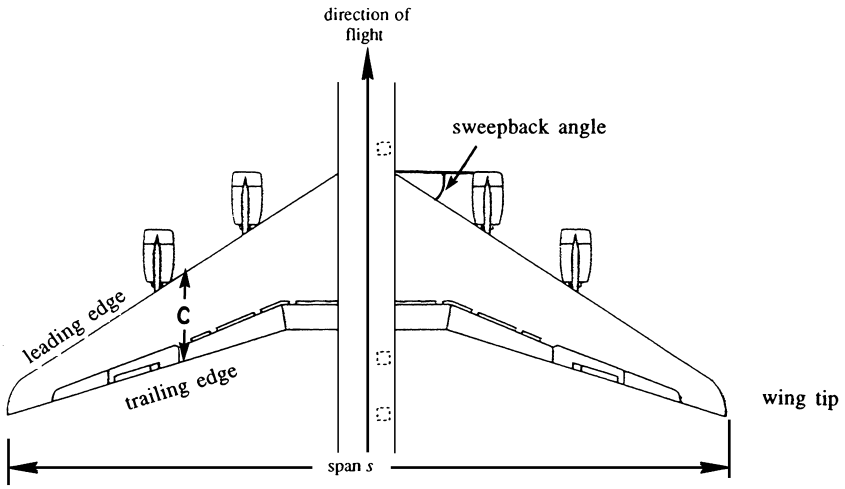

FIGURE 14.2 Wing planform geometry. The span, *s*, is the straight-line distance between wing tips and is shown at the bottom of the figure. The sweepback angle is shown near the starboard wing root. The chord *c* depends on location along the span.

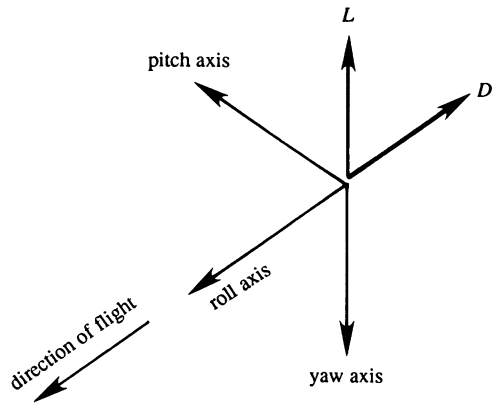

FIGURE 14.3 Aircraft axes. These are defined by the names of aircraft rotations about these axes. Positive pitch raises the aircraft's nose. Positive roll banks the aircraft for a right turn. Positive yaw moves the aircraft's nose to the right from the point of view of the pilot.

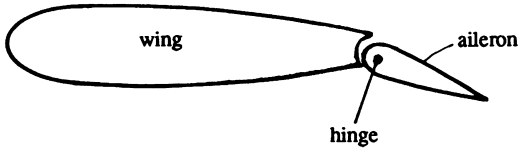

FIGURE 14.4 The aileron. As shown, this aileron deflection would increase lift by increasing the camber of the effective foil shape.

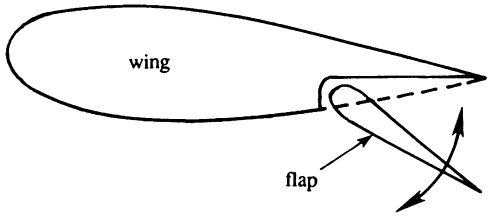

FIGURE 14.5 The flap. As shown, this flat deflection would increase lift by increasing the camber of the effective foil shape. The design of flaps often exploits the flow in the slot formed between the main wing and the rotating flap element to increase lift and delay stall.

Aileron: These are flaps near each wing tip (Figure 14.1), joined to the main wing by a hinged connection, as shown in Figure 14.4. They move differentially in the sense that one moves up while the other moves down. A depressed aileron increases the lift, and a raised aileron decreases the lift, so that a rolling moment results when they are differentially actuated. Ailerons are located near each wing tip to generate a large rolling moment with minimal angular deflection. The pilot generally controls the ailerons by moving a control stick, whose movement to the left or right causes a roll to the left or right. In larger aircraft the aileron motion is controlled by rotating a small wheel that resembles half of an automobile steering wheel.

Elevator: The elevators are hinged to the trailing edge of the horizontal stabilizers (tail fins). Unlike ailerons they move together, and their movement generates a pitching motion of the aircraft. The elevator movements are imparted by the forward and backward movement of a control stick, so that a backward pull lifts the nose of the aircraft.

Rudder: The yawing motion of the aircraft is governed by the hinged rear portion of the vertical tail fin, called the *rudder*. The pilot controls the rudder by pressing his feet against two rudder pedals so arranged that moving the left pedal forward moves the aircraft's nose to the left.

Flap: During takeoff, the speed of the aircraft is too small to generate enough lift to support the weight of the aircraft. To overcome this, a section of the rear of the wing is split, so that it can be rotated downward and moved aft to increase the lift (Figure 14.5). A further function of the flap is to increase both lift and drag during landing.

Modern airliners also have *spoilers* on the top surface of each wing. When raised slightly, they cause early boundary-layer separation on part of the top of the wing and this decreases or *spoils* the wing's lift. They can be deployed together or individually. Reducing the lift on one wing will bank the aircraft so that it will turn in the direction of the lowered wing. When deployed together, overall lift is decreased and the aircraft descends. Spoilers have another function as well. During landing immediately after touchdown, they are deployed fully to eliminate a significant fraction of the aircraft's wing lift and thereby ensure that the aircraft stays on the ground and does not become unintentionally airborne again, even in gusty winds. In addition, the spoilers increase drag and slow the aircraft to shorten the length of its landing roll.

An aircraft is said to be in trimmed flight when there are no moments about its center of gravity and the drag force is minimal. Trim tabs are small adjustable surfaces within or adjacent to the major control surfaces—ailerons, elevators, and rudder. Deflections of these surfaces may be set and held to adjust for a change in the aircraft's center of gravity in flight due to consumption of fuel or a change in the direction of the prevailing wind with respect to the flight path. These are set for steady-level flight on a straight path with minimum deflection of the major control surfaces.

14.3. CHARACTERISTICS OF AIRFOIL SECTIONS

Figure 14.6 shows the shape of the cross section of a wing, called an *airfoil* section (spelled *aerofoil* in the British literature). The leading edge of the profile is generally rounded, whereas the trailing edge is sharp. The straight line joining the centers of curvature of the leading and trailing edges is called the *chord*. The meridian line of the section passing midway between the upper and lower surfaces is called the *camber line*. The maximum height of the camber line above the chord line is called the *camber* of the section. Normally the camber varies from nearly zero for high-speed supersonic wings, to $\approx 5\%$ of chord length for low-speed wings. The angle α between the chord line and the direction of flight (i.e., the direction of the undisturbed stream) is called the *angle of attack* or *angle of incidence*.

The forces on airfoils are usually studied in a foil-fixed frame of reference with a uniform flow approaching the foil along the x-axis with the y-axis pointing vertically upward. The aerodynamic force F on an airfoil can be resolved into a *drag force* D parallel to the oncoming stream, and a *lift force* L perpendicular to the oncoming stream (see Figure 14.7). In steady-level flight the lift equals the weight of the aircraft while its drag is balanced by engine thrust. These forces may be expressed in dimensionless form via the coefficients of lift and drag:

$$C_D \equiv \frac{D}{(1/2)\rho U^2 A}, \quad \text{and} \quad C_L \equiv \frac{L}{(1/2)\rho U^2 A}. \tag{4.107, 4.108}$$

Measurements or specifications of C_D and C_L are the primary means for stating airfoil performance. The drag results from the stress and pressure distributions on the foil's surface. These are called the *friction drag* and the *pressure drag* (or *form drag*), respectively. The lift is almost entirely due to the pressure distribution. Figure 14.8 shows the distribution of the pressure

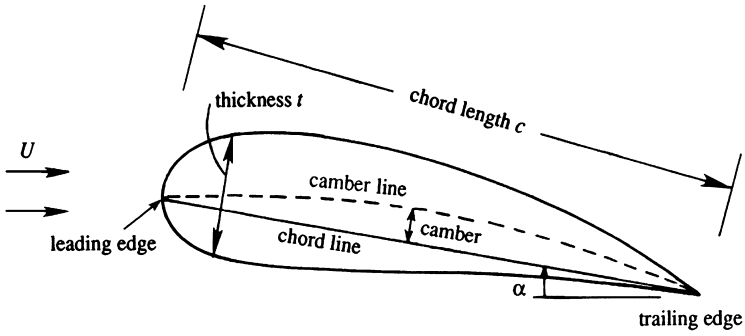

FIGURE 14.6 Airfoil geometry. A rounded leading edge and a sharp trailing edge are essential geometrical features of airfoils. For the material discussed in this chapter, the most important parameters are: the angle of attack α, the chord length c, and the maximum camber. An airfoil's thickness distribution is often modified to minimize drag and/or prevent stall.

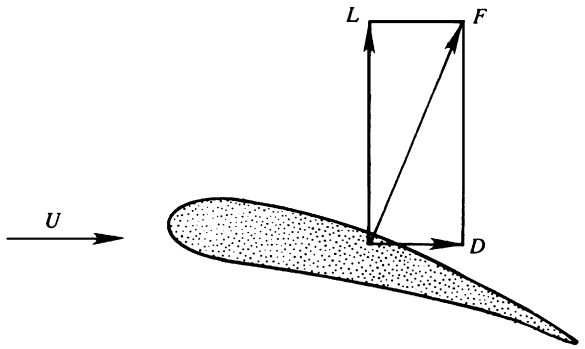

FIGURE 14.7 Forces on an airfoil. Lift L acts perpendicular to the oncoming stream and may be positive or negative. Drag D acts parallel to the oncoming stream and is positive for passive objects.

coefficient $C_p = (p - p_\infty)/(1/2)\rho U^2$ on an airfoil at a moderate angle of attack. The outward arrows correspond to a negative C_p, while a positive C_p is represented by inward arrows. It is seen that the pressure coefficient is negative over most of the surface, except over small regions near the nose and the tail. However, the pressures over most of the upper surface

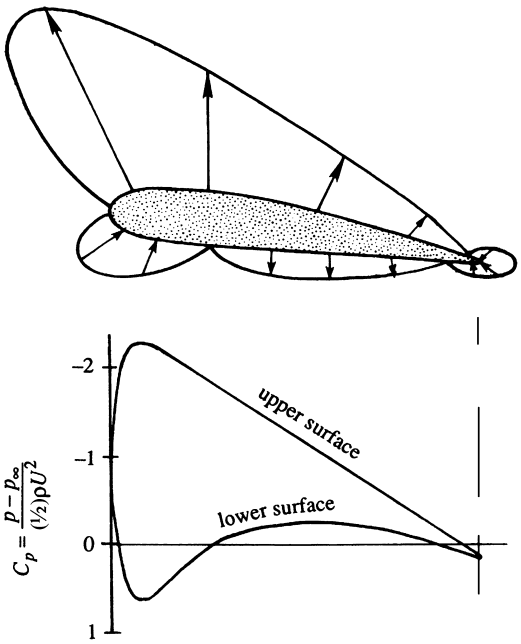

FIGURE 14.8 Distribution of the pressure coefficient C_p over an airfoil. The upper panel shows C_p plotted normal to the surface and the lower panel shows C_p plotted normal to the chord line. Note that negative values appear on the upper half of the vertical axis in the lower panel. And, on the upper or suction foil surface, a pressure minimum occurs near the foil's leading edge. Thus, the suction-side boundary layer faces an adverse pressure gradient over most of the upper surface of the foil.

are smaller than those over the bottom surface, which results in a net lift force. The top and bottom surfaces of an airfoil are popularly referred to as the *suction side* and the *compression* (or *pressure*) *side*, respectively.

In steady ideal flow, the *Kutta-Zhukhovsky lift theorem* (see Section 6.5) requires the lift on a two-dimensional airfoil to be

$$L = \rho U \Gamma, \tag{6.62}$$

where U is the free-stream velocity and Γ is the clockwise circulation around the body. Thus, lift development on an airfoil is synonymous with circulation development. As was seen in Section 6.3 for $0 < \Gamma < 4\pi a U$, the amount of circulation held by a cylinder determines the location of stagnation points where the oncoming stream attaches and separates from the cylinder's surface. This is also true for an airfoil with circulation; foil-surface flow attachment and separation locations are set by the foil's circulation strength. In subsonic aerodynamics, airfoil circulation is determined by the net amount of vorticity trapped in the foil's viscous boundary layers. Thus, asymmetrical foil shapes intended for positive lift generation are designed to place more vorticity in the suction-side boundary layer than in the pressure-side boundary layer. For fixed chord length and free-stream flow speed, three common strategies are followed for robust lift generation and control. The first allows the other two to be effective.

For reliable subsonic lift generation, a foil should have a sharp tailing edge. At low to moderate angles of attack, $|\alpha|$ up to approximately 15° to 20°, a sharp trailing edge causes the suction and pressure side boundary layers to separate together at the foil's trailing edge. Thus, a sharp trailing edge becomes the downstream flow separation point, so its location thereby determines the foil's circulation for a given foil shape and free-stream speed. The actual fluid-dynamic interaction leading to this situation involves the foil's viscous boundary layers and is described later. However, this possibility for controlling circulation was experimentally observed before the development of boundary-layer theory. In 1902, the German aerodynamicist Wilhelm Kutta proposed the following rule: *in flow over a two-dimensional body with a sharp trailing edge, there develops a circulation of magnitude just sufficient to move the rear stagnation point to the trailing edge*. This statement is called the *Kutta condition*, sometimes also called the *Zhukhovsky hypothesis*. It is applied in ideal-flow aerodynamics as a simple means of capturing the viscous flow effects of a foil's attached boundary layers.

A second strategy for controlling a foil's lift is to change its angle of attack α. For $|\alpha| < 15^\circ$ to 20°, increasing α increases the lift, and nominal extreme C_L values from -2 to $+2$ can be obtained from well-designed, single-piece airfoils.

The final strategy for controlling a foil's lift is to change its camber. For a fixed angle of attack, increasing camber increases the lift. This is the primary reason for moveable control surfaces at the trailing edges of the wings and tail fins of an aircraft. Angular rotation of such control surfaces locally changes a foil's camber line and thereby changes the lift force generated by the portion of the wing or fin spanned by the control surface.

Two additional considerations are worth mentioning here. Most foils have a rounded leading edge to keep the foil's suction-side boundary layer attached, and this increases lift and decreases drag. A properly designed leading edge recovers nearly all of the ideal-flow leading edge suction that occurs on foils of negligible thickness (see Exercise 14.7). And, when a foil is pitched upward to a sufficiently high angle of attack, the Kutta condition will fail and the foil's suction-side boundary layer will separate upstream of the foil's trailing

edge. This situation is called *stall* and its onset depends on: the foil's shape, the Reynolds number of the flow, the foil's surface roughness, and other three-dimensional effects. Stall occurs when the suction-side boundary layer cannot overcome the adverse pressure gradient aft of the pressure minimum on the foil's suction side. For small violations of the Kutta condition where the suction-side boundary layer separates at ~80% or 90% of the chord length, a typical foil's lift is not strongly affected but its drag increases. For more severe violations of the Kutta condition, where the suction-side boundary layer separates upstream of the mid-chord location, the foil's lift is noticeably reduced and its drag is greatly increased. In nearly all cases, stall leads to such undesirable foil performance that its onset places important limitations on an aircraft's operating envelope.

The physical reason for the Kutta condition is illustrated in Figure 14.9 where the same simple airfoil and nearby streamlines are shown at three different times. Here, the foil is held fixed and flow is impulsively accelerated to speed U at $t = 0$. Figure 14.9a shows streamlines near the foil immediately after the fluid has started moving but before boundary layers have developed on either its suction or pressure sides. The fluid velocity at this stage has a near discontinuity adjacent to the foil's surface. And, the fluid goes around the foil's trailing edge with a very high velocity and overcomes a steep deceleration and pressure rise from the

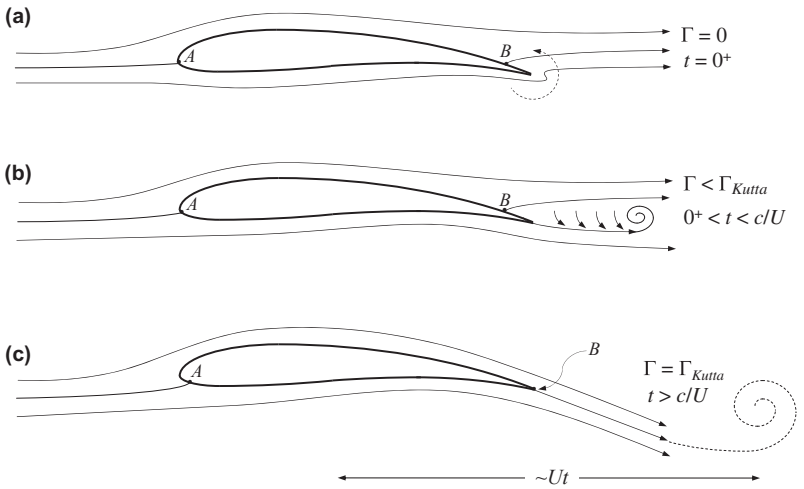

FIGURE 14.9 Flow patterns over a stationary airfoil at a low angle of attack in an impulsively started horizontal flow. (a) Streamlines immediately after the velocity jumps to a positive value. Here the boundary layers on the foil have not had a chance to develop and the rear stagnation (separation) point B occurs on the suction surface of the foil. The foil-surface vorticity at the trailing edge is nearly singular and induces a counterclockwise fluid velocity that draws fluid around the sharp trailing edge. (b) If the pressure-side boundary layer develops first, it will separate from the trailing edge as shown. However, the pressure distribution near the trailing edge and the induced velocities from the foil's near-wake vorticity both act to bring B to the trailing edge. (c) Steady-flow pattern established after the flow has moved a chord length or two. Here the leading edge stagnation point A has moved onto the pressure side of the foil and the net circulation trapped in the foil's boundary layers satisfies the Kutta condition. In this case the rear stagnation (separation) point lies at the foil's trailing edge. The net circulation of the whole flow field remains zero because the unsteady flow process leading to this flow pattern produces a counter-rotating starting vortex, shown in (c) as a dashed spiral.

trailing edge to the rear flow-separation (and -stagnation) point at B. The flow is able to turn the sharp trailing-edge corner because the vorticity on the foil's surface near the trailing edge at this instant is nearly singular at the trailing edge and it induces counterclockwise fluid motion (shown in Figure 14.9a by a dashed arrow). Overall at this time, the flow is irrotational away from the foil's surface, the foil's net circulation is zero, it generates no lift, the forward flow-attachment stagnation point at A is very close to the nose of the foil, and the rear stagnation point at B resides on the foil's suction surface.

Figure 14.9b shows the flow a short time later in a hypothetical situation where the foil's pressure-side boundary layer has developed first. In this case, the points A and B have not moved much. However, the pressure-side boundary layer now separates at the sharp trailing edge because the slowly moving boundary-layer fluid near the foil's surface does not have sufficient kinetic energy to negotiate the steep pressure rise near the stagnation point B nor can it turn the sharp trailing-edge corner. Furthermore, the separated pressure-side boundary-layer flow has carried the near singularity of vorticity, which initially resided on the foil's surface at its trailing edge, into the foil's near wake as a concentrated vortex. Two phenomena near the trailing edge now act to eliminate the zone of separated flow caused by pressure-side boundary-layer separation at the trailing edge. First, the Bernoulli equation ensures that the stagnation pressure at B is higher than the pressure in the moving fluid that is leaving the trailing edge from the pressure side of the foil. The resulting pressure gradient between B and the trailing edge pushes the stationary fluid near B toward the foil's trailing edge. Second, the induced velocities from the vorticity in the separated pressure-side boundary layer and from the near-wake concentrated vortex both induce the stationary fluid near B to move toward the foil's trailing edge. Together these two phenomena cause the rear stagnation point at B to move to the foil's trailing edge. Although an actual impulsively started flow involves simultaneous suction- and pressure-side boundary layer development, the outcome is the same; the rear stagnation point winds up at the trailing edge.

Figure 14.9c shows the final condition after the flow has traveled a chord length or two past the foil. The leading-edge stagnation point has traveled under the nose of the foil and onto the foil's pressure side, and the suction-surface separation point B has been drawn to the foil's trailing edge. (The ideal airfoil trailing edge is a perfect cusp with zero included angle that allows the pressure and suction side flows to meet and separate from the foil without changing direction and without a stagnation point. However, structural requirements cause real foils to have finite included-angle trailing edges, thus point B is a stagnation point even when the trailing edge's included angle is very small; see Section 6.4 and Exercise 14.2.) Once the flow shown in Figure 14.9c is established, the foil now carries more vorticity in its suction-side boundary layer than it does in its pressure-side boundary layer. This difference causes the flow to sweep upward ahead of the foil and downward behind it. The foil's net circulation is that necessary to satisfy the Kutta condition, Γ_{Kutta}. If the foil's circulation is further increased beyond Γ_{Kutta}, the rear stagnation point moves under the foil and onto the *pressure* surface. Although it is an ideal-flow possibility, $\Gamma > \Gamma_{Kutta}$ is not observed in real airfoil flows.

The net circulation in the impulsively started flow described in this section and illustrated in Figure 14.9 is maintained at zero by the presence of an opposite sign vortex, known as a *starting vortex*, in the fluid that was near the foil when the flow began moving. In the scenario described earlier, this vortex is the remnant of the vorticity shed by the pressure-side boundary layer

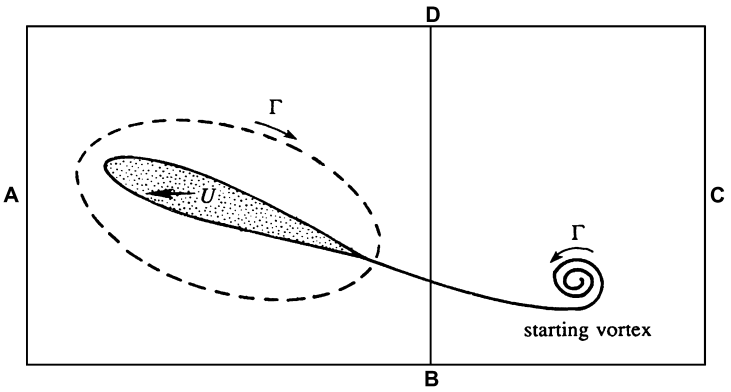

FIGURE 14.10 A material circuit in a stationary fluid that contains an impulsively started airfoil moving to the left. The entire outer part of the circuit was initially in stationary fluid. Thus, the circulation on ABCD must be zero. Therefore, if the sub-circuit ABD contains the airfoil with circulation Γ, then the other sub-circuit BCD must contain a starting vortex with circulation $-\Gamma$.

before point *B* moved to the foil's trailing edge and the cast-off concentrated vorticity that initially caused the flow to fully turn the foil's sharp trailing-edge corner.

The equivalence of the final circulation magnitude bound to the foil and that in the starting vortex is illustrated in Figure 14.10 where the sense of the foil's circulation is clockwise and that in the starting vortex is counterclockwise. For the flow shown in this figure, imagine that the fluid is stationary and the airfoil is moving to the left. Consider a material circuit ABCD large enough to enclose both the initial and final locations of the airfoil. Initially the trailing edge was within the region BCD, which now contains the starting vortex only. According to Kelvin's circulation theorem, the circulation around any material circuit remains constant, if the circuit remains in a region of inviscid flow (although viscous processes may go on *inside* the region enclosed by the circuit). The circulation around the large circuit ABCD therefore remains zero, since it was zero initially. Consequently the counterclockwise circulation of the starting vortex around DBC is balanced by an equal clockwise circulation around ADB. The wing is therefore left with a circulation Γ equal and opposite to the circulation of the starting vortex.

It is clear from the discussion and illustrations in Figure 14.9 that a value of circulation other than Γ_{Kutta} would result a readjustment of the flow. Thus, with every change in flow speed, angle of attack, or airfoil camber (via flap deflection) a new starting vortex is cast off and left behind the foil. A new value of circulation around the airfoil is established to once again place the rear stagnation point at the foil's trailing edge.

Interestingly, *fluid viscosity is not only responsible for the drag, but also for the development of circulation and lift*. In developing the circulation, the flow leads to a steady state where further boundary-layer separation is prevented. The establishment of circulation around an airfoil-shaped body in a real fluid is truly remarkable.

Historical Notes

According to von Karman (1954), the connection between the lift of airplane wings and the circulation around them was recognized and developed by three persons. One of them was the Englishman Frederick Lanchester (1887–1946). He was a multisided and imaginative person, a practical engineer as well as an amateur mathematician. His trade was automobile

building; in fact, he was the chief engineer and general manager of the Lanchester Motor Company. He once took von Karman for a ride around Cambridge in an automobile that he built himself, but von Karman "felt a little uneasy discussing aerodynamics at such rather frightening speed" (p. 34). The second person is the German mathematician Wilhelm Kutta (1867−1944), well known for the Runge-Kutta scheme used in the numerical integration of ordinary differential equations. He started out as a pure mathematician, but later became interested in aerodynamics. The third person is the Russian physicist Nikolai Zhukhovsky, who developed the mathematical foundations of the theory of lift for wings of infinite span, independently of Lanchester and Kutta. An excellent history of flight and the science of aerodynamics is provided by Anderson (1998).

14.4. CONFORMAL TRANSFORMATION FOR GENERATING AIRFOIL SHAPES

In the study of airfoils, one is interested in finding the flow pattern and the surface-pressure distribution. The *direct* solution of the Laplace equation for the prescribed boundary shape of the airfoil is straightforward using a computer, but analytically it is more difficult. In general, analytical solutions are possible only when the airfoil is assumed thin. This is called *thin airfoil theory*, in which the airfoil is replaced by a vortex sheet coinciding with the camber line. An integral equation is developed for the local vorticity distribution from the condition that the camber line be a streamline (velocity tangent to the camber line). The velocity at each point on the camber line is the superposition (i.e., integral) of velocities induced at that point due to the vorticity distribution at all other points on the camber line plus that from the oncoming stream (at infinity). Since the maximum camber is small, evaluations are made on the x-axis of the $x-y$-plane. The Kutta condition is enforced by requiring the strength of the vortex sheet at the trailing edge to be zero. Thin airfoil theory is treated in detail in Kuethe and Chow (1998, Chapter 5) and Anderson (2007, Chapter 4). An *indirect* way to solve the problem involves the method of conformal transformation, in which a mapping function is determined such that the airfoil shape is transformed into a circle. Then a study of the flow around the circle determines the flow pattern around the airfoil. This is called *Theodorsen's method*, which is complicated and will not be discussed here.

Instead, we shall deal with the case in which a *given* transformation maps a circle into an airfoil-like shape and determines the properties of the airfoil generated thereby. This is the *Zhukhovsky transformation*:

$$z = \zeta + \frac{b^2}{\zeta}, \tag{14.3}$$

where b is a constant. It maps regions of the ζ-plane into the z-plane, some examples of which are discussed in Section 6.6. Here, we shall consider circles in different configurations in the ζ-plane and examine their transformed shapes in the z-plane. It will be seen that one of them will result in an airfoil shape.

First consider the transformation of a circle into a straight line. Start from a circle, centered at the origin in the ζ-plane, whose radius b is the same as the constant in the Zhukhovsky transformation (Figure 14.11). For a point $\zeta = be^{i\theta}$ on the circle, the corresponding point in the z-plane is

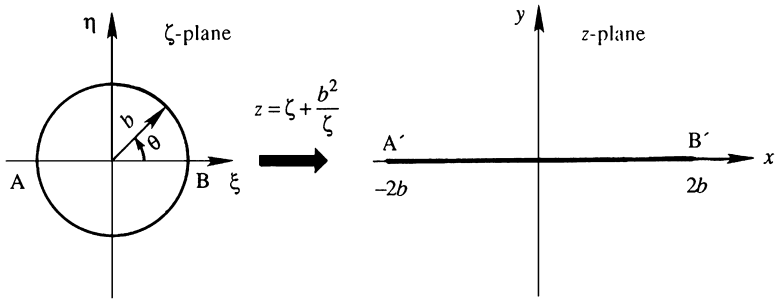

FIGURE 14.11 Transformation of a circle into a straight line. Here the ζ-plane contains the circle of radius b and the transformation $z = \zeta + b^2/\zeta$ converts it into a line segment of length $4b$ in the z-plane.

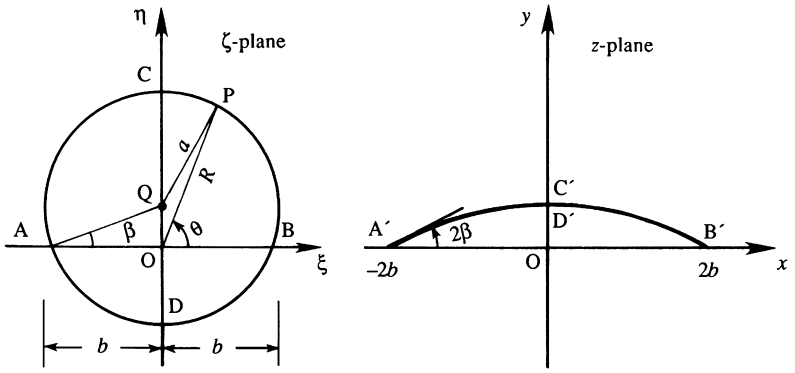

FIGURE 14.12 Transformation of a circle into a circular arc. This situation is similar to that shown in Figure 14.11 except that here the circle is displaced upward and its radius is larger. The object created in the z-plane is a circular arc.

$$z = b\,e^{i\theta} + b\,e^{-i\theta} = 2b\cos\theta.$$

As θ varies from 0 to π, z goes along the x-axis from $2b$ to $-2b$. As θ varies from π to 2π, z goes from $-2b$ to $2b$. The circle of radius b in the ζ-plane is thus transformed into a straight line of length $4b$ in the z-plane. It is clear that the region *outside* the circle in the ζ-plane is mapped into the *entire* z-plane. (It can be shown that the region inside the circle is also transformed into the entire z-plane. This, however, is of no concern to us, since we shall not consider the interior of the circle in the ζ-plane.)

Next consider the transformation of a circle into a circular arc. Again start with a circle in the ζ-plane, but this time let its radius be a ($>b$), let it be centered at point Q along the vertical the η-axis, and let it cut the horizontal ξ-axis at ($\pm b$, 0), as shown in Figure 14.12. If a point on the circle in the ζ-plane is represented by $\zeta = Re^{i\theta}$, then the corresponding point in the z-plane is

$$z = Re^{i\theta} + \frac{b^2}{R}e^{-i\theta},$$

whose real and imaginary parts are:

$$\begin{aligned} x &= (R + b^2/R)\cos\theta, \\ y &= (R - b^2/R)\sin\theta. \end{aligned} \tag{14.4}$$

Eliminating R, we obtain

$$x^2 \sin^2\theta - y^2 \cos^2\theta = 4b^2 \sin^2\theta \cos^2\theta. \tag{14.5}$$

To understand the shape of the curve represented by (14.5) we must express θ in terms of x, y, and the known constants. From triangle OQP, we obtain

$$\mathrm{QP}^2 = \mathrm{OP}^2 + \mathrm{OQ}^2 - 2(\mathrm{OQ})(\mathrm{OP})\cos(\mathrm{Q\widehat{O}P}).$$

Using $\mathrm{QP} = a = b/\cos\beta$ and $\mathrm{OQ} = b\tan\beta$, this becomes

$$\frac{b^2}{\cos^2\beta} = R^2 + b^2\tan^2\beta - 2Rb\tan\beta\cos(90^\circ - \theta),$$

which simplifies to

$$2b\tan\beta\sin\theta = R - b^2/R = y/\sin\theta, \tag{14.6}$$

where (14.4) has been used. We now eliminate θ between (14.5) and (14.6). First note from (14.6) that $\cos^2\theta = (2b\tan\beta - y)/2b\tan\beta$, and $\cot^2\theta = (2b\tan\beta - y)/y$. Then divide (14.5) by $\sin^2\theta$, and substitute these expressions for $\cos^2\theta$ and $\cot^2\theta$. This gives

$$x^2 + (y + 2b\cot 2\beta)^2 = (2b\csc 2\beta)^2,$$

where β is known from $\cos\beta = b/a$. This is the equation of a circle in the z-plane, having the center at $(0, -2b\cot 2\beta)$ and a radius of $2b\csc 2\beta$. The Zhukhovsky transformation has thus mapped a complete circle into a circular arc.

Now consider what happens when the center of the circle in the ζ-plane is displaced to a point Q on the real axis (Figure 14.13). The radius of the circle is again a ($>b$), and we assume that a is slightly larger than b:

$$a \equiv b(1 + e) \qquad e \ll 1. \tag{14.7}$$

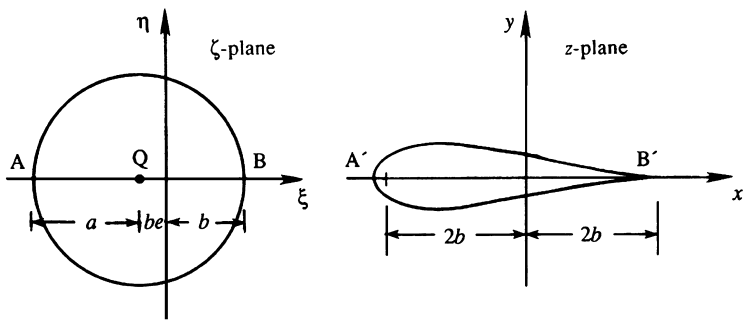

FIGURE 14.13 Transformation of a circle into a symmetric airfoil. This situation is similar to that shown in Figure 14.11 except that here the circle is displaced to the left and its radius is larger. The object created in the z-plane has a symmetric (zero camber) airfoil shape.

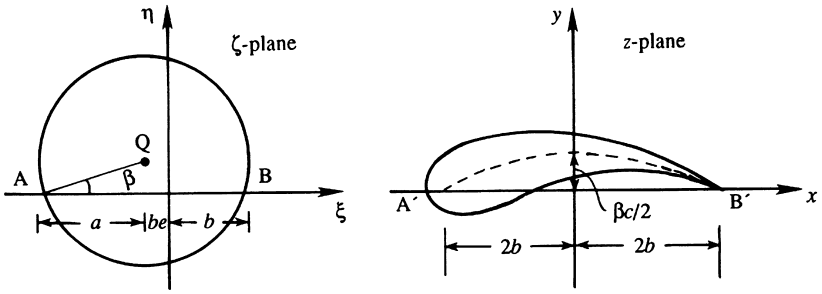

FIGURE 14.14 Transformation of a circle into a cambered airfoil. This situation combines the effects illustrated in Figures 14.11–14.13. The circle is displaced upward and leftward, and its radius is larger. The resulting shape in the z-plane is that of an airfoil.

A numerical evaluation of the Zhukhovsky transformation (14.3), with assumed values for a and b, shows that the corresponding shape in the z-plane is a symmetrical airfoil shape, a streamlined body that is symmetrical about the x-axis. Note that the airfoil in Figure 14.13 has a rounded nose and thickness, while the one in Figure 14.12 has camber but no thickness.

Therefore, a potentially realistic airfoil shape with both thickness and camber can be generated by starting from a circle in the ζ-plane that is displaced in both η and ξ directions (Figure 14.14). The following relations can be proved for $e \ll 1$:

$$c \cong 4b,\ camber = \cong \frac{1}{2}\beta c, \quad \text{and} \quad t_{\max}/c \cong 1.3e. \tag{14.8}$$

Here $t_{\max}$ is the maximum thickness, which is reached nearly at the quarter chord position $x = -b$, and *camber* as defined in Figure 14.6 is indicated in Figure 14.14.

Such airfoils generated from the Zhukhovsky transformation are called *Zhukhovsky airfoils*. They have the property that the trailing edge is a *cusp*, which means that the upper and lower surfaces are tangent to each other at the trailing edge. Without the Kutta condition, the trailing edge is a point of infinite velocity. If the trailing edge angle is nonzero (Figure 14.15a), then a stagnation point occurs at the trailing edge because the suction and pressure side flows must change direction when they meet (Exercise 14.2). However, the cusped trailing edge of a Zhukhovsky airfoil (Figure 14.15b) does not require any flow deflection so it is not a stagnation point. In that case the tangents to the upper and lower surfaces coincide at the trailing edge, and the fluid leaves the trailing edge smoothly. The trailing edge for the Zhukhovsky airfoil is simply an ordinary point where the velocity is neither zero nor infinite.

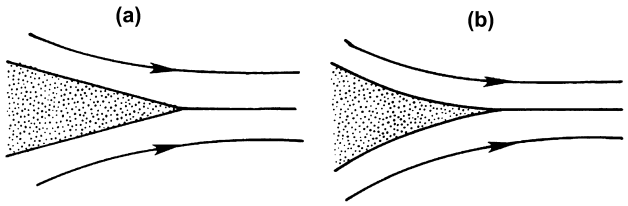

FIGURE 14.15 Shapes of the trailing edge: (a) trailing edge with finite angle; and (b) cusped trailing edge. Application of the Kutta condition to a trailing edge with a finite included angle results in a stagnation point at the trailing edge. A cusped trailing edge avoids the stagnation point.

14.5. LIFT OF A ZHUKHOVSKY AIRFOIL

The preceding section has shown how a circle in the ζ-plane can be transformed into an airfoil in the z-plane with the help of the Zhukhovsky transformation. The performance of such an airfoil can be determined with the aid of the transformation. Start with flow around a circle with clockwise circulation Γ in the ζ-plane, in which the approach velocity is inclined at an angle α with the ξ-axis (Figure 14.16). The corresponding pattern in the z-plane is the flow around an airfoil with circulation Γ and angle of attack α. It can be shown that the circulation does not change during a conformal transformation. If $w = \phi + i\psi$ is the complex potential, then the velocities in the two planes are related by

$$\frac{dw}{dz} = \frac{dw}{d\zeta}\frac{d\zeta}{dz}.$$

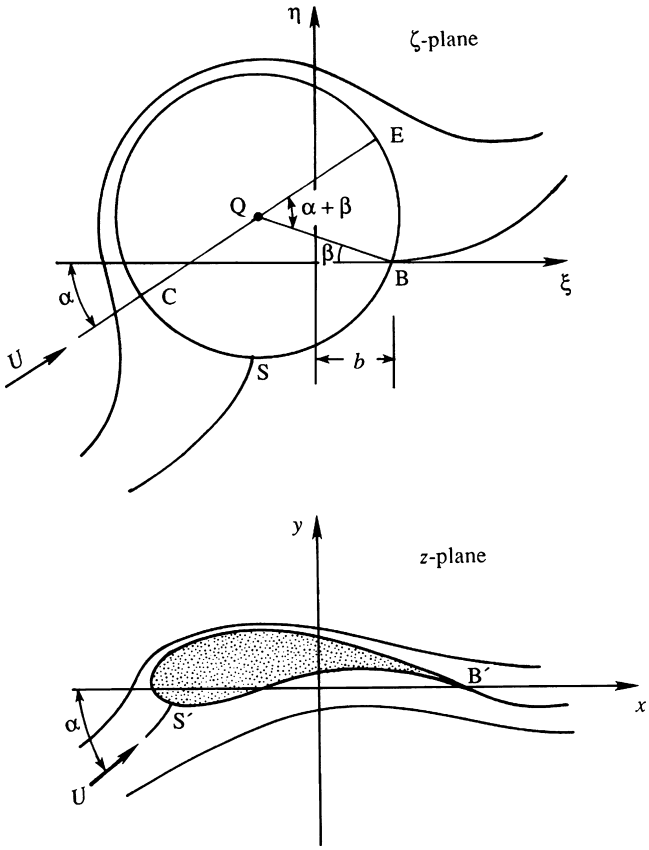

FIGURE 14.16 Transformation of flow around a circle with circulation in the ζ-plane into flow around a Zhukhovsky airfoil in the z-plane. The stagnation points S and B in the upper panel are mapped into the stagnation points S' and B' in the lower panel. The angle of attack α is the same in both complex planes.

Using the Zhukhovsky transformation (14.3), this becomes

$$\frac{dw}{dz} = \frac{dw}{d\zeta}\frac{\zeta^2}{\zeta^2 - b^2}. \tag{14.9}$$

Here $dw/dz = u - iv$ is the complex velocity in the z-plane, and $dw/d\zeta$ is the complex velocity in the ζ-plane. Equation (14.9) shows that the velocities in the two planes become equal as $\zeta \to \infty$, which means that the free-stream velocities are inclined at the same angle α in the two planes.

Point B with coordinates $(b, 0)$ in the ζ-plane is transformed into the trailing edge B′ of the airfoil. Because $\zeta^2 - b^2$ vanishes there, it follows from (14.9) that the velocity at the trailing edge will in general be infinite. If, however, we arrange that B is a stagnation point in the ζ-plane at which $dw/d\zeta = 0$, then dw/dz at the trailing edge will have a zero-over-zero form. Our discussion of Figure 14.15b has shown that this will in fact result in a finite velocity at B′.

From (6.37), the tangential velocity at the surface of the circle in the ζ-plane is given by

$$u_\theta = -2U \sin\theta - \frac{\Gamma}{2\pi a}, \tag{14.10}$$

where θ is measured from the free-stream-aligned diameter CQE. At point B, we have $u_\theta = 0$ and $\theta = -(\alpha + \beta)$. Therefore (14.10) gives

$$\Gamma = 4\pi U a \sin(\alpha + \beta), \tag{14.11}$$

which is the clockwise circulation required by the Kutta condition. It shows that the circulation around an airfoil depends on the speed U, the chord length c ($\simeq 4a$), the angle of attack α, and the camber/chord ratio $\beta/2$. The coefficient of lift is

$$C_L = \frac{L}{(1/2)\,\rho U^2 c} \simeq 2\pi(\alpha + \beta), \tag{14.12}$$

where we have used $4a \simeq c$, $L = \rho U \Gamma$, and $\sin(\alpha + \beta) \simeq (\alpha + \beta)$ for small angles of attack. Equation (14.12) shows that the lift can be increased by adding a certain amount of camber. The lift is zero at a negative angle of attack $\alpha = -\beta$, so that the angle $(\alpha + \beta)$ can be called the *absolute* angle of attack. The fact that the lift of an airfoil is proportional to the angle of attack allows the pilot to control the lift simply by adjusting the attitude (orientation) of the airfoil with respect to its flight direction.

A comparison of the theoretical lift equation (14.12) with typical experimental results for a Zhukhovsky airfoil is shown in Figure 14.17. The small disagreement can be attributed to the finite thickness of the foil-surface boundary layers whose displacement thicknesses change the effective shape of the airfoil. The sudden drop of the lift at $\alpha + \beta \approx 20^\circ$ is the signature of stall, and it is caused by early suction-side boundary-layer separation that worsens with increasing angle of attack. Stall is further discussed in Section 14.7.

Zhukhovsky airfoils are not practical for two basic reasons. First, they demand a cusped trailing edge, which cannot be practically constructed or maintained. Second, the camber line in a Zhukhovsky airfoil is nearly a circular arc, and therefore the maximum camber lies close to the center of the chord. However, a maximum camber within the forward portion of the chord is usually preferred so as to obtain a desirable pressure distribution. To get

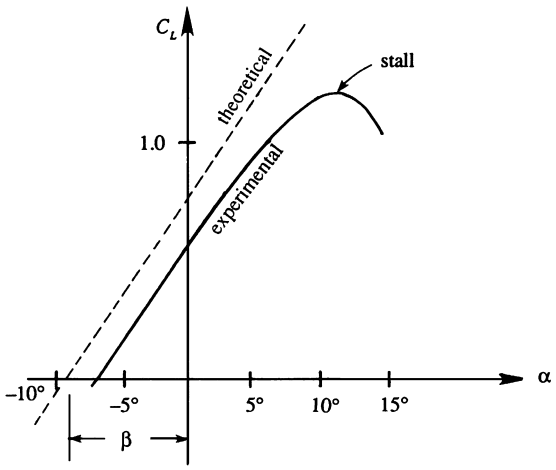

FIGURE 14.17 Comparison of theoretical and experimental lift coefficients for a cambered Zhukhovsky airfoil. The lift curve slopes match well and boundary-layer thicknesses may account for the offset between theoretical and measured curves. The most important difference is that the real airfoil stalls while the ideal one does not.

around these difficulties, other families of airfoils have been generated from circles by means of more complicated transformations. Nevertheless, the results for a Zhukhovsky airfoil given here have considerable application as reference values, and the conformal mapping technique remains an efficient means for assessing airfoil designs.

14.6. ELEMENTARY LIFTING LINE THEORY FOR WINGS OF FINITE SPAN

The foregoing two-dimensional results apply only to wings of infinite span. However, many of the concepts of two-dimensional aerodynamics can be extrapolated to three-dimensional flow and wings of finite span when the vorticity shed from a three-dimensional wing is accounted for. The lifting line theory of Prandtl and Lanchester is the simplest means for accomplishing this task and it provides useful insights into how lift and drag develop on finite span wings. Lifting line theory is based on several approximations to the three-dimensional flow field of a finite wing, so our starting point is a description of such a flow.

Figure 14.18 shows a schematic view of a finite-span wing, looking downstream from the aircraft. As the pressure on the lower surface of the wing is greater than that on the upper surface, air flows around the wing tips from the lower into the upper side. Therefore, there is a span-wise component of velocity toward the wing tip on the underside of the wing and toward the wing root on the upper side, as shown by the streamlines in Figure 14.19a. The span-wise momentum acquired as the fluid passes the wing continues into the wake downstream of the trailing edge. On the stream surface extending downstream from the wing, therefore, the lateral component of the flow is outward (toward the wing tips) on the underside and inward on the upper side. On this surface, then, there is vorticity oriented in the stream-wise direction. This stream-wise vorticity has opposite signs on the two sides of

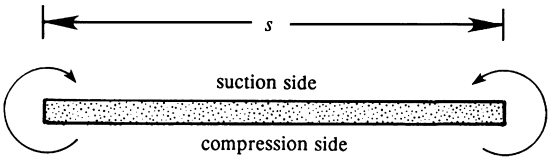

FIGURE 14.18 Flow around wing tips. Low suction-side pressures and high pressure-side pressures cause fluid to move toward the wing tips on the underside of a finite wing, and to move away from the wing tips on the topside of a finite wing. This three-dimensional flow eventually produces the tip vortices.

the wing-center axis OQ. The stream-wise vortex filaments downstream of the wing are called *trailing vortices*, which form a *vortex sheet* (Figure 14.19b) in the near wake of the wing. As discussed in Section 5.8, a vortex sheet is composed of closely spaced vortex filaments that generate a discontinuity in tangential velocity.

Downstream of the wing, each half of the vortex sheet rolls up on itself and forms two distinct counter-rotating vortices called *tip vortices* (Figure 14.20). The circulation of each tip vortex is equal to Γ_0, the circulation at the center of the wing. Tip vortices may become visually evident when an aircraft flies in humid air. The decreased pressure (due to the high velocity) and temperature in the core of the tip vortices may cause atmospheric moisture to condense into droplets or ice crystals, which may be seen in the form of *vapor trails* extending for many kilometers behind an aircraft traversing a clear sky. This textbook's cover shows the trailing-vortex-induced distortion of a cloud layer behind a commercial airliner. Here the aircraft's mass is more than 100,000 kilograms. Thus, the strength of its trailing vortices is sufficient to cause substantial cloud motion on a scale comparable to the aircraft's wingspan. As an aircraft proceeds after takeoff, the tip vortices get longer, which means that kinetic energy is being constantly supplied to generate them. Thus, an additional drag force must be experienced by a wing of finite span. This is called the *induced drag*, and it can be predicted with lifting line theory.

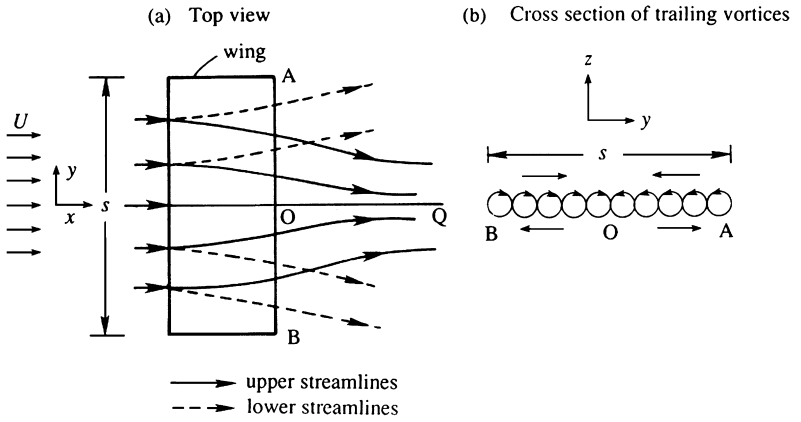

FIGURE 14.19 Flow over a wing of finite span: (a) top view of streamline patterns on the upper and lower surfaces of the wing; and (b) cross section of trailing vortices behind the wing. The trailing vortices change sign at O, the center of the wing.

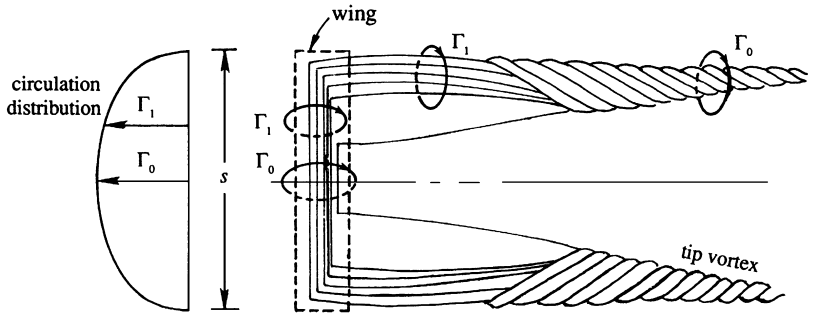

FIGURE 14.20 Rolling up of trailing vortices to form tip vortices. The mutual interaction of the trailing vortices eventually produces two counter-rotating wing-tip vortices having the same circulation as that bound to the center of the main wing. The effect of such vortices on a cloud layer is shown on the cover of this textbook.

One of Helmholtz's vortex theorems states that a vortex filament cannot end in the fluid, but must either end at a solid surface or form a closed vortex loop or ring. In the case of the finite wing, the tip vortices are the extension of the vorticity trapped in the wing's boundary layers. The tip vortices start at the wing and are joined together downstream of the aircraft by the various starting vortices of the wing. Starting vortices are left behind at the point where the aircraft took off and where the wing's lift was changed for aircraft maneuvers (ascent, descent, turns, etc.). In any case, the starting vortices are usually so far behind the wing that their effect on the wing's performance may be neglected and the tip vortices may be regarded as extending an infinite distance aft of the wing.

Three assumptions are needed for the simple version of lifting line theory presented here. The first is that the wing's aspect ratio, span/(average chord), is so large that the flow at any span-wise location may be treated as two dimensional. A second assumption is that the actual physical structure of the aircraft does not matter and that the aircraft's main wing may be replaced by a single (straight) vortex segment of variable strength. This vortex segment is called the *bound vortex*. It moves with the aircraft and lies along the aircraft's wings, nominally located at the center of lift at any span-wise location along the wing. The bound vortex forms the *lifting line* segment from which the theory draws its name. In general, the bound vortex is strongest near the midspan and weakest near the wing tips. According to one of the Helmholtz theorems (Section 5.3), a vortex cannot begin or end in the fluid; it must end at a wall or form a closed loop. Therefore, as the bound vortex weakens from wing root to wing tip it releases vortex filaments that turn parallel to the stream-wise direction and are advected downstream, eventually coalescing to form the tip vortices. A third assumption made in lifting line theory is that the interaction of these trailing vortex filaments with each other can be ignored. Thus, each trailing vortex filament starts at the bound vortex and is assumed to lie along a straight semi-infinite horizontal line parallel to the upstream flow direction. Although a formal mathematical account of the theory was first published by Prandtl, many of the important underlying ideas were first conceived by Lanchester. The historical controversy regarding the credit for the theory is noted at the end of this section.

With these assumptions and the geometry shown in Figure 14.21, a relation can be derived between the distribution of circulation along the wingspan and the strength of the trailing vortex filaments. Suppose that the clockwise circulation of the bound vortex changes from

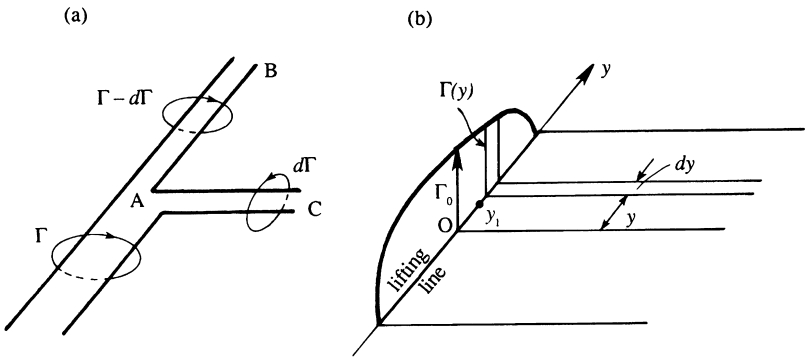

FIGURE 14.21 The mechanism leading to trailing vortices. (a) When the bound vortex having strength Γ weakens, it sheds a vortex filament AC of strength $d\Gamma$ into the wing's wake and continues along the wing as the vortex AB with strength $\Gamma - d\Gamma$. (b) The shed vortex filament that leaves the bound vortex at location y induces a downward velocity at location y_1 of the bound vortex when $y > y_1$. The induced velocity from all trailing vortex filaments is known as *downwash*.

Γ to $\Gamma - d\Gamma$ at a certain point (Figure 14.21a). Then another vortex AC of strength $d\Gamma$ must emerge from the location of the change. In fact, the strength and sign of the circulation around AC is such that, when AC is folded back onto AB, the circulation is uniform along the composite vortex tube. (Recall the vortex theorem of Helmholtz, which says that the strength of a vortex tube is constant along its length.) Now consider the vortex strength or circulation distribution $\Gamma(y)$ that represents the main wing (Figure 14.21b). The change in circulation in length dy is $d\Gamma$, which is a decrease if $dy > 0$. It follows that the magnitude of the trailing vortex filament of width dy is $-(d\Gamma/dy)dy$. For simple wings, the trailing vortices will be stronger near the wing tips where $d\Gamma/dy$ is the largest.

The critical contribution of lifting line theory is that it allows an approximate means of assessing the impact of the trailing vortex filaments on the performance of the bound vortex representing the aircraft's wing. The simplest means of assessing this impact is to determine the velocity induced at a point y_1 on the lifting line by the trailing vortex filament that leaves the wing at location y, and then integrating over the trailing filament contributions from all possible y values. Based on the Biot-Savart law (5.17), a straight semi-infinite trailing vortex filament that leaves the wing at y with strength $-(d\Gamma/dy)dy$ and remains horizontal induces a downward velocity of magnitude:

$$dw(y_1) = \frac{-(d\Gamma/dy)dy}{4\pi(y - y_1)}$$

at location y ($< y_1$) along the lifting line (Exercise 14.10 with $\theta_1 = 0$ and $\theta_2 = 90°$). This velocity increment is *half* the velocity induced by an infinitely long vortex element. The bound vortex does not induce a velocity on itself, so for a wing of span s, the total downward velocity at y_1 due to the entire trailing vortex sheet is therefore

$$w(y_1) = \frac{1}{4\pi}\int_{-s/2}^{s/2} \frac{d\Gamma}{dy}\frac{dy}{(y_1 - y)}, \tag{14.13}$$

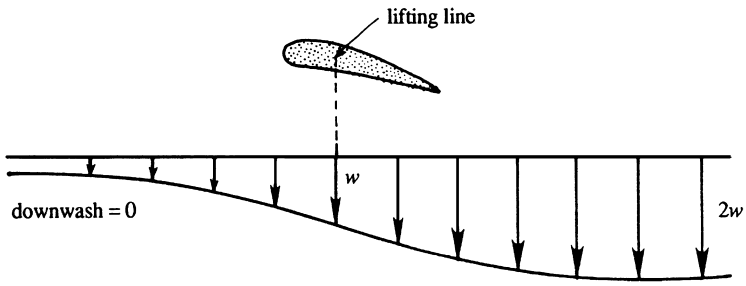

FIGURE 14.22 Variation of downwash ahead of and behind an airfoil. The downwash is weaker upstream of the wing and stronger downstream of it. The actual profile can be determined from the Biot-Savart law (see (5.17) and Exercise 14.10).

which is called the *downwash* at y_1 on the lifting line. The vortex sheet also induces a smaller downward velocity in front of the airfoil and a larger one behind the airfoil (Figure 14.22).

This downwash velocity adds to the free-stream velocity so that the incident flow at any location along the wing is the vector resultant of U and w (Figure 14.23). The downwash therefore changes the local angle of attack of the airfoil, decreasing it by the angle

$$\varepsilon = \tan\frac{w}{U} \simeq \frac{w}{U},$$

where the approximate equality follows when $w \ll U$, the most common situation in applications. Thus, the *effective angle of attack* at any span-wise location is

$$\alpha_e = \alpha - \varepsilon = \alpha - \frac{w}{U}. \tag{14.14}$$

Because the aspect ratio is assumed large, ε is assumed to be small. Each element dy of the finite wing may then be assumed to act as though it is an isolated two-dimensional section set in a stream of uniform velocity U_e, at an angle of attack α_e. According to the Kutta-Zhukhovsky lift theorem, a circulation Γ superimposed on the actual resultant velocity U_e generates an elemental aerodynamic force $dL_e = \rho U_e \Gamma dy$, which acts normal to U_e. This force

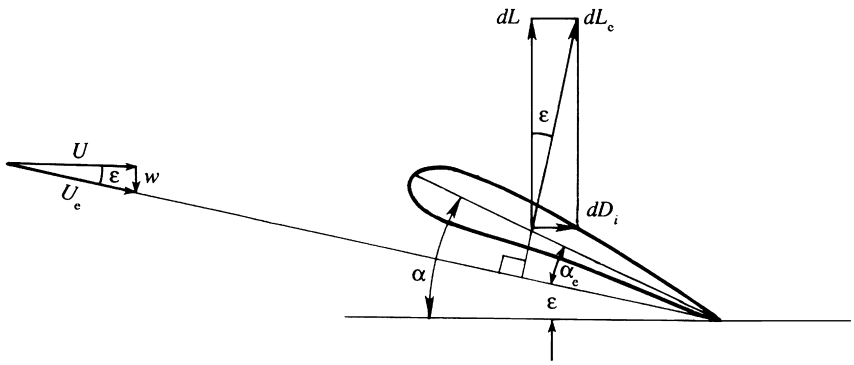

FIGURE 14.23 Lift and lift-induced drag on a wing element dy in the presence of a downwash velocity w. The downwash velocity locally lowers the angle of attack of the free stream and rotates the lift vector backward to produce the lift-induced drag.

may be resolved into two components, the conventional lift force $d\mathrm{L}$ normal to the direction of flight and a component dD_i parallel to the direction of flight (Figure 14.23). Therefore

$$dL = dL_\mathrm{e} \cos\varepsilon = \rho U_\mathrm{e}\Gamma\, dy \cos\varepsilon \simeq \rho U\Gamma\, dy,$$
$$dD_\mathrm{i} = dL_\mathrm{e} \sin\varepsilon = \rho U_\mathrm{e}\Gamma\, dy \sin\varepsilon \simeq \rho w\Gamma\, dy.$$

In general w, Γ, U_e, ε, and α_e are all functions of y, so that for the entire wing:

$$L = \int_{-s/2}^{s/2} \rho U\Gamma\, dy,$$
$$D_\mathrm{i} = \int_{-s/2}^{s/2} \rho w\Gamma\, dy. \tag{14.15}$$

These expressions have a simple interpretation: whereas the interaction of U and Γ generates L, which acts normal to U, the interaction of w and Γ generates D_i, which acts normal to w.

The drag force D_i induced by the trailing vortices is called the *induced drag* and is zero for a wing of infinite span. It arises on a wing of finite span because it continuously creates trailing vortices and the rate of generation of trailing-vortex kinetic energy must equal the rate of work done against the induced drag, namely $D_\mathrm{i}U$. For this reason, the induced drag is also known as the *vortex drag*. It is analogous to the *wave drag* experienced by a ship, which continuously radiates gravity waves during its motion. As we shall see, the induced drag is the largest part of the total drag experienced by an airfoil (away from stall).

A basic reason why there must be a downward velocity behind the wing is the following: The fluid exerts an upward lift force on the wing, and therefore the wing exerts a downward force on the fluid. The fluid must therefore constantly gain downward momentum as it goes past the wing.

For a given $\Gamma(y)$, $w(y)$ can be determined from (14.13) and D_i can then be determined from (14.15). However, $\Gamma(y)$ itself depends on the distribution of $w(y)$ because the effective angle of attack is changed due to $w(y)$. To see how $\Gamma(y)$ may be estimated, first note that the lift coefficient for a two-dimensional Zhukhovsky airfoil is nearly $C_L = 2\pi\,(\alpha + \beta)$. For a finite wing we may assume

$$C_L = K\left[\alpha - \frac{w(y)}{U} + \beta(y)\right], \tag{14.16}$$

where $(\alpha - w/U)$ is the effective angle of attack, $-\beta(y)$ is the angle of attack for zero lift (found from experimental data such as Figure 14.17), and K is the lift-curve slope, a constant whose value is nearly six for most airfoils ($K = 2\pi$ for Zhukhovsky and thin airfoils). An expression for the circulation can be obtained by noting that the lift coefficient is related to the circulation as $C_L = L/((1/2)\rho U^2 c) = \Gamma/((1/2)Uc)$, so that $\Gamma = (1/2)UcC_L$. Equation (14.16) is then equivalent to the assumption that the circulation for a wing of finite span is

$$\Gamma(y) = \frac{K}{2}Uc(y)\left[\alpha - \frac{w(y)}{U} + \beta(y)\right]. \tag{14.17}$$

For a given $U, \alpha, c(y)$, and $\beta(y)$, (14.13) and (14.17) define an integral equation for determining $\Gamma(y)$.

An approximate solution to these two equations can be obtained by changing y and y_1 to angular variables γ and γ_1:

$$y = -(s/2)\cos\gamma \quad \text{and} \quad y_1 = -(s/2)\cos\gamma_1,$$

so that $\gamma = 0$ and $\gamma = \pi$ correspond to the left (port) and right (starboard) wing tips, respectively, and then assuming a Fourier series form for the circulation strength of the lifting line:

$$\Gamma = \sum\nolimits_{n=1}^{\infty} \Gamma_n \sin(n\gamma), \tag{14.18}$$

where the Γ_n are undetermined coefficients. When (14.18) is substituted into (14.13), the resulting equation is:

$$w(y_1) = \frac{1}{2\pi s}\int_0^{\pi} \sum_{n=1}^{\infty} n\Gamma_n \frac{\cos(n\gamma)d\gamma}{\cos\gamma_1 - \cos\gamma} = \frac{1}{2\pi s}\sum_{n=1}^{\infty} n\Gamma_n \int_0^{\pi} \frac{\cos(n\gamma)d\gamma}{\cos\gamma_1 - \cos\gamma} = \frac{1}{2s}\sum_{n=1}^{\infty} n\Gamma_n \frac{\sin(n\gamma_1)}{\sin\gamma_1}, \tag{14.19}$$

where the final equality comes from evaluating the integral. Combing (14.17) through (14.19) and dropping the subscript "1" from γ, produces a single equation for the coefficients Γ_n:

$$\frac{K}{2}Uc(\alpha + \beta) = \sum_{n=1}^{\infty}\left(1 + \frac{nKc}{4s\sin\gamma}\right)\Gamma_n \sin(n\gamma), \tag{14.20}$$

where K, c, α, and β may all be functions of the transformed span coordinate γ. Thus, (14.20) is not a typical Fourier series solution because the coefficients of $\sin(n\gamma)$ inside the sum depend on γ. In practice, (14.20) can be solved approximately by truncating the sum after N terms, and then requiring its validity at N points along the wing to convert it into N algebraic equations for Γ_1, Γ_2, … Γ_N. Fortunately in many circumstances, just a few terms in the sum are needed to adequately represent $\Gamma(y)$.

With an approximate solution for $\Gamma(y)$ provided by several Γ_n computed algebraically from (14.20), the wing's lift and induced drag computed from (14.15) are:

$$L = \frac{\pi s}{4}\rho U\Gamma_1, \quad \text{and} \quad D_i = \frac{\pi}{8}\rho\sum_{n=1}^{N} n\Gamma_n^2. \tag{14.21, 14.22}$$

Thus, the wing's performance is maximized when $\Gamma_1 \neq 0$ and $\Gamma_n = 0$ for all $n > 1$, because this produces the maximum lift-to-drag ratio. In this case (14.18) reduces to:

$$\Gamma = \Gamma_1\sin(\gamma) = \Gamma_1\sqrt{1 - (2y/s)^2}, \tag{14.23}$$

which is known as an *elliptical lift distribution*. The downwash for an elliptical lift distribution is constant across the wingspan,

$$w(y) = \Gamma_1/2s, \tag{14.24}$$

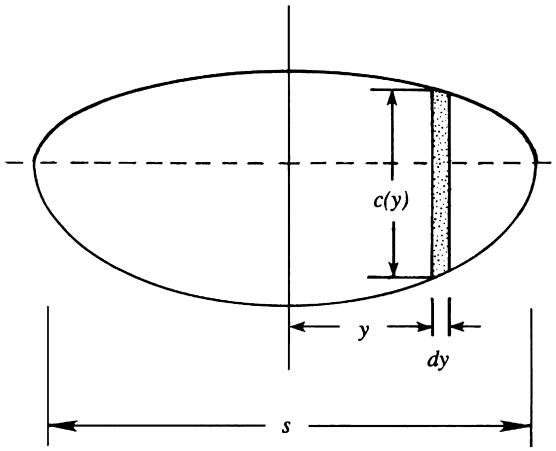

FIGURE 14.24 Wing with an elliptic planform. Here the variation in the chord over the span can produce an elliptical lift distribution. This planform is similar to that of the *British Spitfire*, a WWII combat aircraft.

as can be found from substituting (14.23) into (14.19). The induced drag for an elliptical lift distribution is

$$D_i = \frac{\pi}{8}\rho\Gamma_1^2 = \frac{2L^2}{\pi\rho U^2 s^2}, \tag{14.25}$$

where (14.21) has been used to introduce L in the second equality. Thus, the induced drag coefficient for an elliptical lift distribution is:

$$C_{D_i} = \frac{D_i}{(1/2)\rho U^2 A} = \frac{C_L^2}{\pi(s^2/A)} = \frac{C_L^2}{\pi\Lambda}, \tag{14.26}$$

where C_L and C_D are given by (4.107) and (4.108) in Section 4.3, A is the wing's planform area, and Λ is the wing's aspect ratio. Equation (14.26) shows that $C_{D_i} \to 0$ when the flow is two dimensional, that is, in the limit $\Lambda \to \infty$. More importantly, it shows that the *induced drag coefficient increases as the square of the lift coefficient*. We shall see in the following section that the induced drag generally makes the largest contribution to the total drag of an airfoil.

Since an elliptic circulation distribution minimizes the induced drag, it is of interest to determine the circumstances under which such a circulation can be established. Consider an element dy of the wing (Figure 14.24). The lift on the element is:

$$dL = \rho U\Gamma\, dy = C_L\frac{1}{2}\rho U^2 c\, dy, \tag{14.27}$$

where $c dy$ is a wing area element. If the circulation distribution is elliptic, then the downwash is independent of y. In addition, if the wing profile is geometrically similar at every point along the span and has the same geometrical angle of attack α, then the effective angle of

attack and hence the lift coefficient C_L will be independent of y. Equation (14.27) shows that the chord length c is then simply proportional to Γ, and so $c(y)$ is also elliptically distributed. Thus, an untwisted wing with elliptic planform, or composed of two semi-ellipses (Figure 14.24), will generate an elliptic circulation distribution. However, the same effect can also be achieved with nonelliptic planforms if the angle of attack varies along the span, that is, if the wing has twist (see Exercise 14.14).

The results of lifting line theory have had an enormous impact on the design and development of subsonic aircraft. However, the results presented here are approximate because of the geometrical assumptions made about the aircraft's wings, its trailing vortices, and the tip vortices. Thus, an elliptical lift distribution is only approximately optimal, and a more general theory would produce refinements. Yet, with suitable geometric modifications lifting line theory can be applied to multiple-wing aircraft and rotating propellers. Furthermore, its implications help explain near-ground effects for landing aircraft, and the Λ-pattern commonly formed by flocks of migrating birds.

Lanchester Versus Prandtl

There is some controversy in the literature about who should get more credit for developing lifting line theory. Since Prandtl in 1918 first published the theory in a mathematical form, textbooks for a long time have called it the *Prandtl Lifting Line Theory*. Lanchester was bitter about this, because he felt that his contributions were not adequately recognized. The controversy has been discussed by von Karman (1954, p. 50), who witnessed the development of the theory. He gives a lot of credit to Lanchester, but falls short of accusing his teacher Prandtl of being deliberately unfair. Here we shall note a few facts that von Karman brings up.

Lanchester was the first person to study a wing of finite span. He was also the first person to conceive that a wing can be replaced by a bound vortex, which bends backward to form the tip vortices. Last, Lanchester was the first to recognize that the minimum power necessary to fly is that required to generate the kinetic energy field of the downwash field. It seems, then, that Lanchester had conceived all of the basic ideas of the wing theory, which he published in 1907 in the form of a book called *Aerodynamics*. In fact, a figure from his book looks very similar to the current Figure 14.20.

Many of these ideas were explained by Lanchester in his talk at Göttingen, long before Prandtl published his theory. Prandtl, his graduate student von Karman, and Carl Runge were all present. Runge, well known for his numerical integration scheme of ordinary differential equations, served as an interpreter, because neither Lanchester nor Prandtl could speak the other's language. As von Karman said, "both Prandtl and Runge learned very much from these discussions."

However, Prandtl did not want to recognize Lanchester for priority of ideas, saying that he conceived of them before he saw Lanchester's book. Such controversies cannot be settled, and great intellects have been involved in controversies before.

In view of the fact that Lanchester's book was already in print when Prandtl published his theory, and the fact that Lanchester had all the ideas but not a formal mathematical theory, we have called it the *Lifting Line Theory of Prandtl and Lanchester* at the outset of this section.

14.7. LIFT AND DRAG CHARACTERISTICS OF AIRFOILS

Before an aircraft is built its wing design is tested in a wind tunnel, and the results are generally given as plots of C_L and C_D versus the angle of attack α. A typical plot is shown in Figure 14.25 where it is seen that, for $-4^\circ < \alpha < 12^\circ$, the variation of C_L with α is approximately linear, a typical value of $dC_L/d\alpha$ $(= K)$ being ≈ 0.1 per degree. The lift reaches a maximum value at $\alpha \approx 15^\circ$. If the angle of attack is increased further, the steep adverse pressure gradient on the upper surface of the airfoil causes the flow to separate before reaching the wing's trailing edge, and a large wake is formed (Figure 14.26). The drag coefficient increases and the lift coefficient drops. The wing is said to *stall* as the suction-side boundary-layer separation point moves toward the leading edge. Beyond the stalling incidence angle the lift coefficient levels off again and remains at $\approx 0.7-0.8$ up to α values of 10s of degrees.

For a fixed-shape wing, the maximum possible lift coefficient depends largely on the Reynolds number Re. For chord-based Reynolds numbers of $\mathrm{Re} \sim 10^5-10^6$, the suction-side

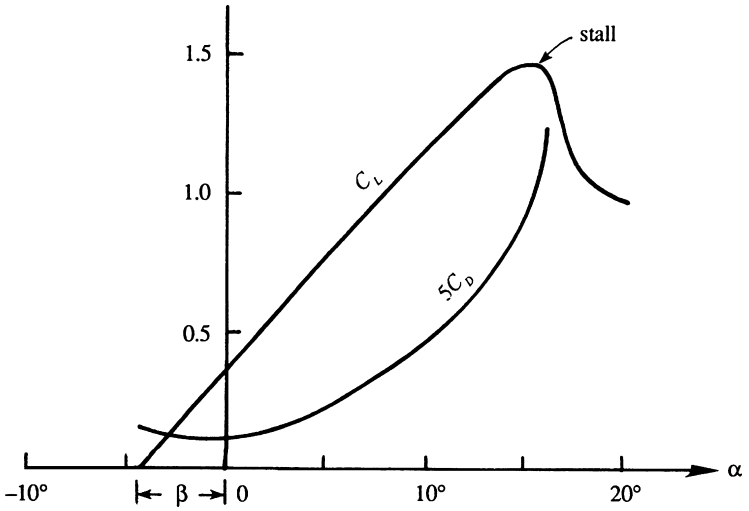

FIGURE 14.25 Generic lift and drag coefficients vs. angle of attack. There is lift at $\alpha = 0$ so the foil shape has nonzero camber. The drag increase is almost quadratic with increasing angle of attack in accordance with (14.26).

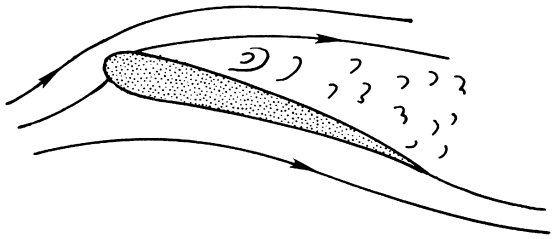

FIGURE 14.26 Stalling of an airfoil. Here the Kutta condition is no longer satisfied, and the flow separates near the leading edge on the foil's suction side. In this situation, the foil's lift and drag are comparable.

boundary layer may separate before it undergoes transition, and stall may begin before α reaches 10° leading to maximum lift coefficients < 0.9. At larger Reynolds numbers, say $\mathrm{Re} > 10^7$, the suction-side boundary layer transitions to turbulence before it separates and is therefore able to stay attached up to α-values approaching or exceeding 20°. Maximum lift coefficients near or even slightly above two may be obtained at the highest Reynolds numbers.

The angle of attack at zero lift, denoted by $-\beta$ here, is a function of the airfoilsection's camber. (For a Zhukhovsky airfoil, $\beta = 2(\text{camber})/\text{chord}$.) The effect of increasing the airfoil camber is to raise the entire graph of C_L versus α, thus increasing the maximum values of C_L without stalling. A cambered profile delays stall because its leading edge points into the airstream while the rest of the airfoil is inclined to the stream. Rounding the airfoil nose is also essential, since an airfoil of zero thickness would undergo separation at the leading edge. Trailing edge flaps act to increase the camber and thereby the lift coefficient when they are deployed, and this allows lower aircraft landing speeds.

Various terms are in common usage to describe the different components of the drag. The total drag of a body can be divided into a *friction drag* due to the tangential stresses on the surface and *pressure drag* due to the normal stresses. The pressure drag can be further subdivided into an *induced drag* and a *form drag*. The induced drag is the drag that results from the work done by the body to supply the kinetic energy of the downwash field as the trailing vortices increase in length. The form drag is defined as the part of the total pressure drag that remains after the induced drag is subtracted out. (Sometimes the skin friction and form drags are grouped together and called the *profile drag*, which represents the drag due to the wing's geometrical profile alone and not due to the finiteness of the wing.) The form drag depends strongly on the shape and orientation of the airfoil and can be minimized by good design. In contrast, relatively little can be done about the induced drag if the wing's aspect ratio is fixed.

Normally the induced drag constitutes the major part of the total drag of a wing. As C_{D_i} is nearly proportional to C_L^2, and C_L is nearly proportional to α, it follows that $C_{D_i} \propto \alpha^2$. This is why the drag coefficient in Figure 14.25 seems to increase quadratically with angle of attack.

For high-speed aircraft, the appearance of shock waves can adversely affect the behavior of the lift and drag characteristics. In such cases the maximum *flow* speeds can be close to or higher than the speed of sound even when the aircraft is flying at subsonic speeds. Shock waves can form when the local flow speed exceeds the local speed of sound. To reduce their effect, the wings are given a *sweepback angle*, as shown in Figure 14.2. The maximum flow speeds depend primarily on the component of the oncoming stream perpendicular to the leading edge; this component is reduced as a result of the sweepback. Thus, increased flight speeds are achievable with highly swept wings. This is particularly true when the aircraft flies at supersonic speeds in which there is invariably a shock wave in front of the nose of the fuselage, extending downstream in the form of a cone. Highly swept wings are then used in order that the wing does not penetrate this shock wave. For flight speeds exceeding Mach numbers of order 2, the wings have such large sweepback angles that they resemble the Greek letter Δ; these wings are sometimes called *delta wings*.

14.8. PROPULSIVE MECHANISMS OF FISH AND BIRDS

The propulsive mechanisms of many animals are based on lift generation by wing-like surfaces. Just the basic ideas of this interesting subject are presented here. More detail is provided by Lighthill (1986).

First consider swimming fish. They develop *forward* thrust by horizontally oscillating their tails from *side to side*. Fish tails like that shown in Figure 14.27a have a cross section resembling that of a symmetric airfoil. One-half of the oscillation is represented in Figure 14.27b, which shows the top view of the tail. The sequence 1 to 5 represents the positions of the tail during the tail's motion to the left. A quick change of *orientation* occurs at one extreme position of the oscillation during 1 to 2; the tail then moves to the left during 2 to 4, and another quick change of orientation occurs at the other extreme during 4 to 5.

Suppose the tail is moving to the left at speed V, and the fish is moving forward at speed U. The fish controls these magnitudes so that the resultant fluid velocity U_r (relative to the tail) is inclined to the tail surface at a positive angle of attack. The resulting lift L is perpendicular to U_r and has a forward component $L \sin \theta$. (It is easy to verify that there is a similar forward propulsive force when the tail moves from left to right.) This thrust, working at the rate $UL \sin \theta$, propels the fish. To achieve this propulsion, the tail of the fish pushes sideways on the water against a force of $L \cos \theta$, which requires work at the rate $VL \cos \theta$. Since $V/U = \tan \theta$, the conversion of energy is ideally perfect—all of the oscillatory work done by the fish tail goes into the translation. In practice, however, this is not the case because of the presence of induced drag and other effects that generate a wake.

Most fish stay afloat by controlling the buoyancy of an internal swim bladder. In contrast, some large marine mammals such as whales and dolphins develop *both* a forward thrust and a vertical lift by moving their tails *vertically*. They are able to do this because their tail surface is *horizontal*, in contrast to the vertical tail shown in Figure 14.27. A review by Fish and Lauder (2006) provided evidence that leading-edge tubercles as seen on humpback whale flippers increase lift and reduce drag at high angles of attack. This is because separation is

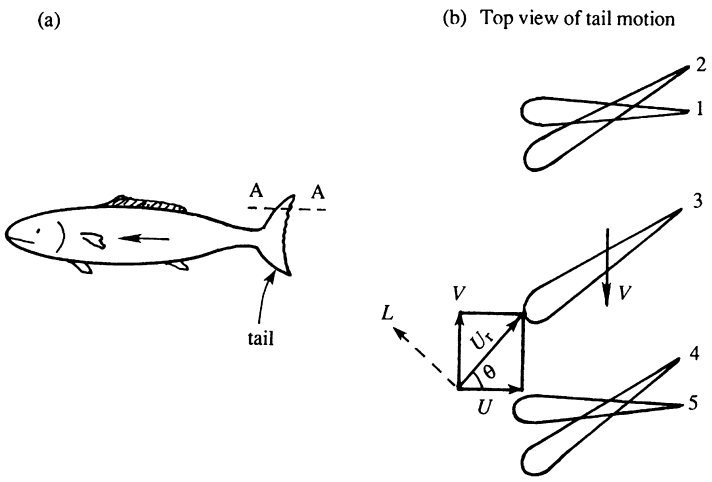

FIGURE 14.27 Propulsion of fish. (a) The cross section of the tail along AA is that of a symmetric airfoil. Five positions of the tail during its motion to the left are shown in (b). The lift force L is normal to the resultant speed U_r of water with respect to the tail.

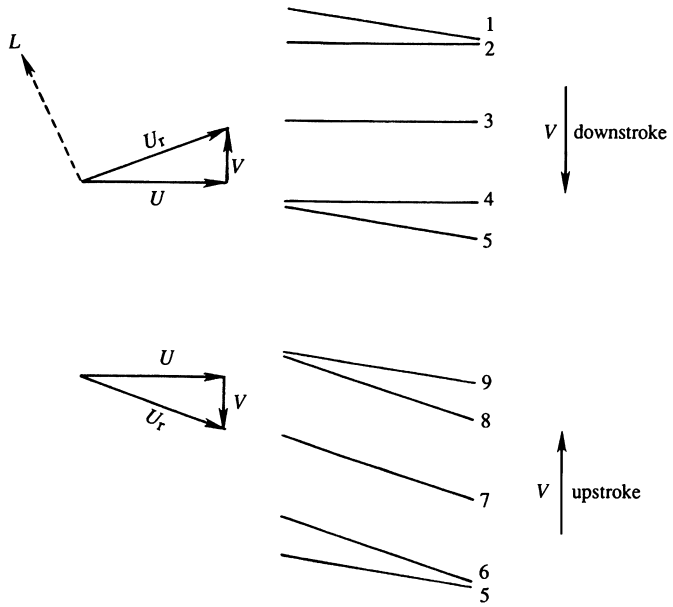

FIGURE 14.28 Propulsion of a bird. A cross section of the wing is shown during upstroke and downstroke. During the downstroke, a lift force L acts normal to the resultant speed U_r of air with respect to the wing. During the upstroke, U_r is nearly parallel to the wing and very little aerodynamic force is generated.

delayed due to the creation of stream-wise vortices on the suction side. Cetacean flukes or flippers and fish tail fins as well as dorsal and pectoral fins are flexible and can vary their camber during a stroke. As a result they are very efficient propulsive devices.

Now consider flying birds, who flap their wings to generate *both* the lift to support their body weight and the forward thrust to overcome drag. Figure 14.28 shows a vertical section of the wing positions during the upstroke and downstroke of the wing. (Birds have cambered wings, but this is not shown in the figure.) The angle of inclination of the wing with the airstream changes suddenly at the end of each stroke, as shown. The important point is that the upstroke is inclined at a greater angle to the airstream than the downstroke. As the figure shows, the downstroke develops a lift force L perpendicular to the resultant velocity of the air relative to the wing. Both a forward thrust and an upward force result from the downstroke. In contrast, very little aerodynamic force is developed during the upstroke, as the resultant velocity is then nearly parallel to the wing. Birds therefore do most of the work necessary for flight during the downstroke.

Liu et al. (2006) provide the most complete description to date of wing planform, camber, airfoil section, and span-wise twist distribution of seagulls, mergansers, teals, and owls. Moreover, flapping as viewed by video images from free flight was digitized and modeled by a two-jointed wing at the quarter chord point. The data from this paper can be used to model the aerodynamics of bird flight.

Using previously measured kinematics and experiments on an approximately 100-times upscaled model, Ramamurti and Sandberg (2001) calculated the flow about a Drosophila

(fruit fly) in flight. They matched Reynolds number (based on wing-tip speed and average chord) and found that viscosity had negligible effect on thrust and drag at a flight Reynolds number of 120. The wings were near elliptical plates with axis ratio 3:1.2 and thickness about 1/80 of the span. Averaged over a cycle, the mean thrust coefficient (thrust/[dynamic pressure $\times$ wing surface]) was 1.3 and the mean drag coefficient close to 1.5.

14.9. SAILING AGAINST THE WIND

People have sailed without the aid of an engine for thousands of years and have known how to reach an upwind destination. Actually, it is not possible to sail exactly against the wind, but it is possible to sail at $\approx 40-45^\circ$ to the wind. Figure 14.29 shows how this is made possible by the aerodynamic lift on the sail, which is a piece of stretched and stiffened cloth. The wind speed is U, and the sailing speed is V, so that the apparent wind speed relative to the boat is U_r. If the sail is properly oriented, this gives rise to a lift force perpendicular to U_r and a drag force parallel to U_r. The resultant force F can be resolved into a driving component (thrust) along the motion of the boat and a lateral component. The driving component performs work in moving the boat; most of this work goes into overcoming the frictional drag and in generating the gravity waves that radiate outward from the hull. The lateral component does not cause much sideways drift because of the shape of the hull. It is clear that the thrust decreases as the angle θ decreases and normally vanishes when θ is $\approx 40-45^\circ$. The energy for sailing comes from the wind field, which loses kinetic energy after passing the sail.

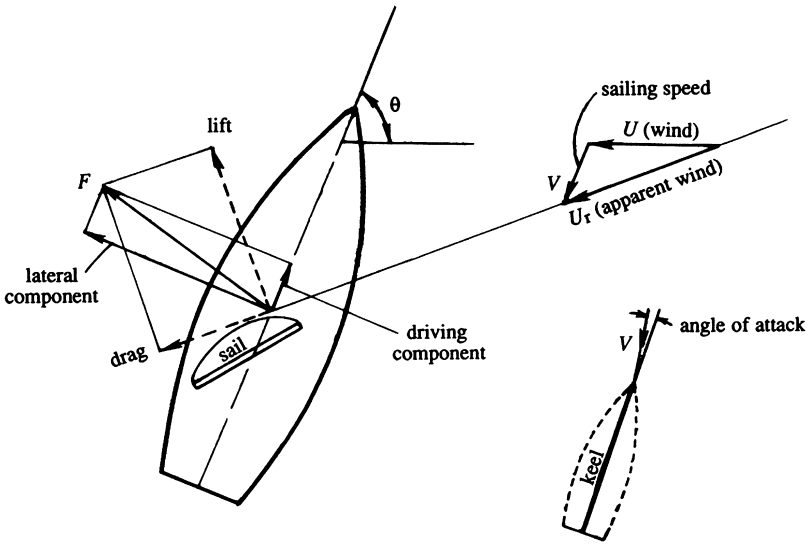

FIGURE 14.29 Principle of sailing against the wind. A small component of the sail's lift pushes the boat forward at an angle $\theta < 90^\circ$ to the wind. Thus by traversing a zig-zag course at angles $\pm\theta$, a sailboat can reach an upwind destination. A sailboat's keel may make a contribution to its upwind progress too.

In the foregoing discussion we have not considered the hydrodynamic forces exerted by the water on the hull. At constant sailing speed the net hydrodynamic force must be equal and opposite to the net aerodynamic force on the sail. The hydrodynamic force can be decomposed into a drag (parallel to the direction of motion) and a lift. The lift is provided by the sailboat's *keel*, which is a thin vertical surface extending downward from the bottom of the hull. For the keel to act as a lifting surface, the longitudinal axis of the boat points at a small angle to the direction of motion of the boat, as indicated near the bottom right part of Figure 14.29. This keel-angle of attack is generally $< 3^\circ$ and is not noticeable. The hydrodynamic lift developed by the keel opposes the aerodynamic lateral force on the sail. It is clear that without the keel the lateral aerodynamic force on the sail would topple the boat around its longitudinal axis.

To arrive at a destination directly against the wind, one has to sail in a zig-zag path, always maintaining an angle of $\approx 45^\circ$ to the wind. For example, if the wind is coming from the east, we can first proceed northeastward as shown, then change the orientation of the sail to proceed southeastward, and so on. In practice, a combination of a number of sails is used for effective maneuvering. The mechanics of sailing yachts is discussed in Herreshoff and Newman (1966).

EXERCISES

14.1. Consider the elementary aerodynamics of a projectile of mass m with $C_L = 0$ and $C_D =$ constant. In Cartesian coordinates with gravity g acting downward along the y-axis, a set of equations for such a projectile's motion are:

$$m\frac{dV_x}{dt} = -D\cos\theta, m\frac{dV_y}{dt} = -mg - D\sin\theta, \tan\theta = V_y/V_x, \text{ and } D = \frac{1}{2}\rho\left(V_x^2 + V_y^2\right)AC_D,$$

where V_x and V_y are the horizontal and vertical components of the projectile's velocity, θ is the angle of the projectile's trajectory with respect to the horizontal, D is the drag force on the projectile, ρ is the air density, and A is projectile's frontal area. Assuming a shallow trajectory, where $V_x^2 \gg V_y^2$ and $mg \gg D\sin\theta$, show that the distance traveled by the projectile over level ground is: $x \cong \dfrac{2m}{\rho AC_D}\ln\left(1 + \dfrac{\rho AC_D V_o^2\cos\theta_o\sin\theta_o}{mg}\right)$ if it is launched from ground level with speed of V_o at an angle of θ_o with respect to the horizontal. Does this answer make sense as $C_D \to 0$?

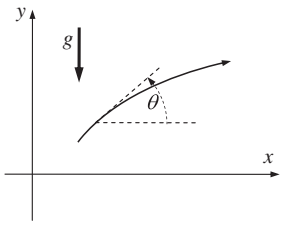

14.2. As a model of a two-dimensional airfoil's trailing edge flow, consider the potential $\phi(r,\theta) = (Ud/n)(r/d)^n\cos(n\theta)$in the usual r-θ coordinates (Figure 3.3a). Here U, d, and

n are positive constants, the fluid has density ρ, and the foil's trailing edge lies at the origin of coordinates.

a) Sketch the flow for $n = 3/2$, $5/4$, and $9/8$ in the angle range $|\theta| < \pi/n$, and determine the full included angle of the foil's trailing edge in terms of n.

b) Determine the fluid velocity at $r = d$ and $\theta = 0$.

c) If p_0 is the pressure at the origin of coordinates and p_d is the pressure at $r = d$ and $\theta = 0$, determine the pressure coefficient: $C_p = (p_0 - p_d)/(1/2)\rho U^2$ as a function of n. In particular, what is C_p when $n = 1$ and when $n > 1$?

14.3. Consider an airfoil section in the xy-plane, the x-axis being aligned with the chord line. Examine the pressure forces on an element $d\mathbf{s} = (dx, dy)$ on the surface, and show that the net force (per unit span) in the y-direction is

$$F_y = -\int_0^c p_u \, dx + \int_0^c p_1 \, dx,$$

where p_u and p_1 are the pressure on the upper and the lower surfaces and c is the chord length. Show that this relation can be rearranged in the form

$$C_y \equiv \frac{F_y}{(1/2)\rho U^2 c} = \oint C_p d\left(\frac{x}{c}\right),$$

where $C_p = (p_0 - p_\infty)/(1/2)\rho U^2$, and the integral represents the area enclosed in a C_p versus x/c diagram, such as Figure 14.8. Neglect shear stresses. [Note that C_y is not exactly the lift coefficient, since the airstream is inclined at a small angle α with respect to the x-axis.]

14.4. The measured pressure distribution over a section of a two-dimensional airfoil at 4° incidence has the following form:
Upper Surface: C_p is constant at -0.8 from the leading edge to a distance equal to 60% of chord and then increases linearly to 0.1 at the trailing edge.
Lower Surface: C_p is constant at -0.4 from the leading edge to a distance equal to 60% of chord and then increases linearly to 0.1 at the trailing edge.
Using the results of Exercise 14.3, show that the lift coefficient is nearly 0.32.

14.5. The Zhukhovsky transformation $z = \zeta + b^2/\zeta$ transforms a circle of radius b, centered at the origin of the ζ-plane, into a flat plate of length $4b$ in the z-plane. The circulation around the cylinder is such that the Kutta condition is satisfied at the trailing edge of the flat plate. If the plate is inclined at an angle α to a uniform stream U, show that:

(i) The complex potential in the ζ-plane is $w = U(\zeta e^{-i\alpha} + 1/\zeta b^2 e^{i\alpha}) + \dfrac{i\Gamma}{2\pi} ln\,(\zeta e^{-i\alpha})$, where $\Gamma = 4\pi Ub \sin\alpha$. Note that this represents flow over a circular cylinder with circulation in which the oncoming velocity is oriented at an angle α.

(ii) The velocity components at point P $(-2b, 0)$ in the ζ-plane are $\left[\frac{3}{4}U\cos\alpha, \frac{9}{4}U\sin\alpha\right]$.

(iii) The coordinates of the transformed point P′ in the xy-plane are $[-5b/2, 0]$.

(iv) The velocity components at $[-5b/2, 0]$ in the xy-plane are $[U\cos\alpha, 3U\sin\alpha]$.

14.6. In Figure 14.12, the angle at A′ has been marked 2β. Prove this. [*Hint*: Locate the center of the circular arc in the z-plane.]

14.7. Ideal flow past a flat plate inclined at angle α with respect to a horizontal free stream produces lift but no drag when the Kutta condition is applied at the plate's trailing edge. However, pressure forces can only act in the plate-normal direction and this direction is *not* perpendicular to the flow. Therefore, to achieve zero drag, another force must act on the plate. This extra force is known as *leading-edge suction* and its existence can be assessed from the potential for flow around the tip of a flat plate that is coincident with the x-axis for $x > 0$. In two-dimensional polar coordinates, this velocity potential is $\phi = 2U_o\sqrt{ar}\cos(\theta/2)$ where U_o and a are velocity and length scales, respectively, that characterize the flow.

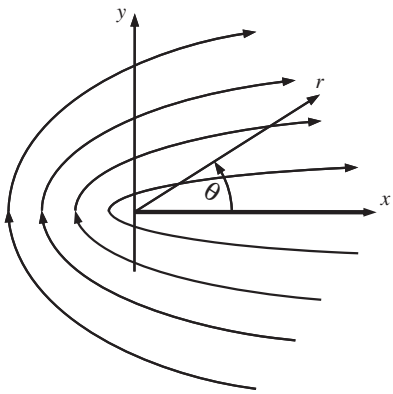

a) Determine u_r and u_θ, the radial and angular-directed velocity components, respectively.

b) If the pressure far from the origin is p_∞, determine the pressure p at any location (r, θ).

c) Use the given potential, a circular control volume of radius ε centered at the origin of coordinates, and the control volume version of the ideal flow momentum equation, $\int_C \rho\mathbf{u}(\mathbf{u}\cdot\mathbf{n})d\xi = -\int_C p\mathbf{n}d\xi + \mathbf{F}$, to determine the force $\mathbf{F}$ (per unit depth into the page) that holds the plate stationary when $\varepsilon \to 0$. Here, $\mathbf{n}$ is the outward unit normal vector to the control volume surface, and $d\xi$ is the length increment of the circular control surface.

d) If the plate is released from rest, in what direction will it initially accelerate?

14.8. Consider a cambered Zhukhovsky airfoil determined by the following parameters: $a = 1.1$, $b = 1.0$, and $\beta = 0.1$. Using a computer, plot its contour by evaluating the Zhukhovsky transformation. Also plot a few streamlines, assuming an angle of attack of 5°.

14.9. A thin Zhukhovsky airfoil has a lift coefficient of 0.3 at zero incidence. What is the lift coefficient at 5° incidence?

14.10. Lifting line theory involves calculating vortex-induced velocities from the Biot-Savart induction law, (5.17). Consider an idealized vortex segment of uniform strength Γ that lies along the z-axis between z_1 and z_2, and has a sense of rotation that points along the z-axis. In this case the induced velocity $\mathbf{u}$ at the location (R, φ, z) will be given by the integral:

$$\mathbf{u}(\mathbf{x},t) = \int_{z_1}^{z_2} d\mathbf{u} = \frac{\Gamma}{4\pi}\int_{z_1}^{z_2} \mathbf{e}_z \times \frac{(\mathbf{x}-\mathbf{x}')}{|\mathbf{x}-\mathbf{x}'|^3} dz'.$$

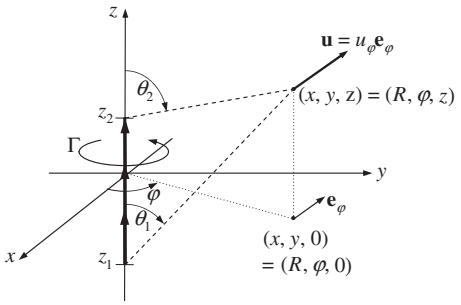

a) Evaluate this integral to show that $\mathbf{u}(\mathbf{x},t) = (\Gamma/4\pi R)(\cos\theta_1 - \cos\theta_2)\mathbf{e}_\varphi$ where the angles θ_1 and θ_2 are defined in the figure.

b) Show that the velocity induced by an infinite ideal-line vortex is recovered from the part a) result for an appropriate choice of angles.

c) What is the induced velocity on the z-axis ($R = 0$) when $z < z_1$ or $z > z_2$?

14.11.[1] The simplest representation of a three-dimensional aircraft wing in flight is the rectangular horseshoe vortex.

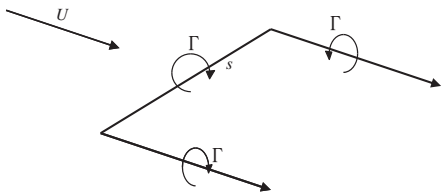

a) Calculate the induced downwash at the center of the wing.

b) Assuming the result of part a) applies along the entire wingspan, estimate C_{D_i}, the lift-induced coefficient of drag, in terms of the wing's aspect ratio: $AR = s^2/A$, and the wing's coefficient of lift $C_L = L/(1/2)\rho U^2 A$, where A is the planform area of the wing.

c) Explain why the result of part b) appears to surpass the performance of the optimal elliptic lift distribution.

14.12. The circulation across the span of a wing follows the parabolic law $\Gamma = \Gamma_0(1 - (2y/s)^2)$. Calculate the induced velocity w at midspan, and compare the value with that obtained when the distribution is elliptic.

14.13. An untwisted elliptic wing of 20-m span supports a weight of 80,000 N in a level flight at 300 km/hr. Assuming sea level conditions, find a) the induced drag and b) the circulation around sections halfway along each wing.

14.14.[1] A wing with a rectangular planform (span $= s$, chord $= c$) and uniform airfoil section without camber is twisted so that its geometrical angle, α_w, decreases from α_r at the root ($y = 0$) to zero at the wing tips ($y = \pm s/2$) according to the distribution: $\alpha_w(y) = \alpha_r\sqrt{1 - (2y/s)^2}$.

a) At what global angle of attack, α_t, should this wing be flown so that it has an elliptical lift distribution? The local angle of attack at any location along the span will be $\alpha_t + \alpha_w$. Assume the two-dimensional lift curve slope of the foil section is K.

b) Evaluate the lift and the lift-induced drag forces on the wing at the angle of attack determined in part a) when: $\alpha_r = 2°$, $K = 5.8$ rad.$^{-1}$, $c = 1.5$ m, $s = 9$ m, the air density is 1 kg/m^3, and the airspeed is 150 m/s.

14.15. Consider the wing shown in Figure 14.24. If the foil section is uniform along the span and the wing is not twisted, show that the three-dimensional lift coefficient, $C_{L,3D}$ is related to the two-dimensional lift coefficient of the foil section, $C_{L,2D}$, by: $C_{L,3D} = C_{L,2D}/(1 + 2/\Lambda)$, where $\Lambda = s^2/A$ is the aspect ratio of the wing.

14.16. The wing-tip vortices from large, heavy aircraft can cause a disruptive rolling torque on smaller, lighter ones. Lifting line theory allows the roll torque to be estimated when the small airplane's wing is modeled as a single linear vortex with strength $\Gamma(y)$that resides at $x = 0$ between $y = -s/2$ and $y = +s/2$. Here, the small airplane's wing will be presumed rectangular (span s, chord c) with constant foil-shape, and the trailing vortex from the heavy airplane's wing will be assumed to lie along the x-axis and produce a vertical velocity distribution at $x = 0$ given by: $w(y) = \dfrac{\Gamma'}{2\pi y}[1 - \exp(-|y|/\ell)]$. To simplify your work for the following items, ignore the trailing vortices (shown as dashed lines) from the small airplane's wing and assume $U \gg w$. [Note this w differs by a sign from that specified in (14.17).]

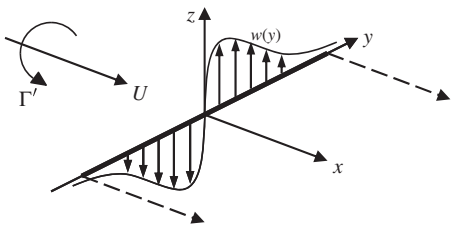

a) Determine a formula for the rolling moment, $M = \int_{-s/2}^{+s/2} \rho U y \Gamma(y) dy$, on the small aircraft's wing in terms of Γ', s, c, ℓ, the air density ρ, the flight speed of the small aircraft U, and the lift-curve slope of the small aircraft's wing section $K = dC_{L,2D}/d\alpha$, where α is the small-aircraft-wing angle of attack.

[1]Obtained by the third author while a student in a course taught by Professor Fred Culick.

b) Calculate M when $\rho = 1.2$ kg/m^3, $U = 150$ m/s, $K = 6.0$/rad, $s = 9$ m, $c = 1.5$ m, $\Gamma' = 50$ m^2/s, and $s/(2\,\ell) = 1$. Comment on the magnitude of this torque.

14.17. Consider the ideal rectilinear horseshoe vortex of a simple wing having span s. Use the (x, y, z) coordinates shown for the following items.

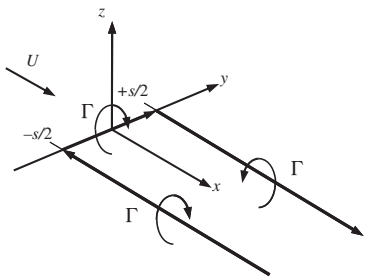

a) Determine a formula for the induced vertical velocity w at $(x, y, 0)$ for $x > 0$ and $y > 0$.

b) Using the results of part a), evaluate the induced vertical velocity at the following three locations: $(s, 0, 0)$, $(0, s, 0)$, and $(s, s, 0)$.

c) Imagine that you are an efficiency-minded migrating bird and that the rectilinear horseshoe vortex shown is produced by another member of your flock. Describe where you would choose to center your own wings. List the coordinates of the part b) location that is closest to your chosen location.

14.18. As an airplane lands, the presence of the ground changes the plane's aerodynamic performance. To address the essential features of this situation, consider uniform flow past a horseshoe vortex (heavy solid lines below) with wingspan b located a distance h above a large, flat boundary defined by $z = 0$. From the method of images, the presence of the boundary can be accounted for by an image horseshoe vortex (heavy dashed lines below) of opposite strength located a distance h below the boundary.

a) Determine the direction and the magnitude of the induced velocity at $\mathbf{x} = (0, 0, h)$, the center of the wing.

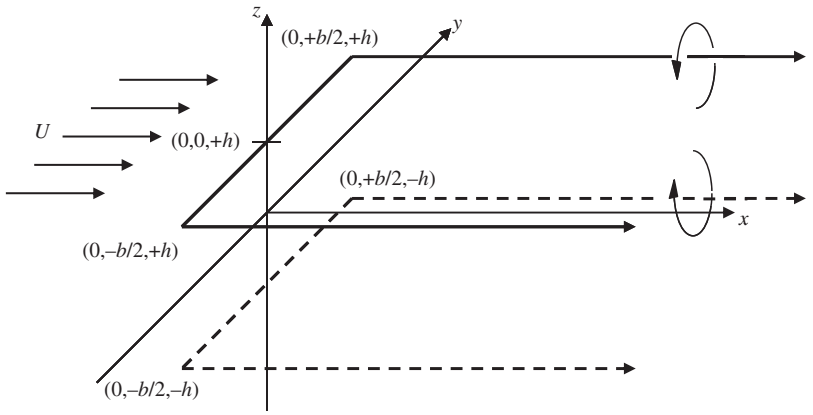

b) Assuming the result of part a) applies along the entire wingspan, estimate L and D_i, the lift and lift-induced drag, respectively, in terms of b, h, Γ, and ρ = fluid density.

c) Compare the result of part b) to that obtained for the horseshoe vortex without a large, flat surface: $L = \rho U \Gamma b$ and $D_i = \rho \Gamma^2 / \pi$. Which configuration has more lift? Which one has less drag? Why?

14.19. Before modifications, an ordinary commercial airliner with wingspan $s = 30$ m generates two tip vortices of equal and opposite circulation having Rankine velocity profiles (see (3.28)) and a core size $\sigma_o = 0.5$ m for test-flight conditions. The addition of wing-tip treatments (sometimes known as *winglets*) to both of the aircraft's wing tips doubles the tip vortex core size at the test condition. If the aircraft's weight is negligibly affected by the change, has the lift-induced drag of the aircraft been increased or decreased? Justify your answer. Estimate the percentage change in the induced drag.

Literature Cited

Anderson, John D., Jr. (1998). *A History of Aerodynamics*. London: Cambridge University Press.

Anderson, John D., Jr. (2007). *Fundamentals of Aerodynamics*. New York: McGraw-Hill.

Fish, F. E., & Lauder, G. V. (2006). Passive and Active Control by Swimming Fishes and Mammals. *Annual Rev. Fluid Mech, 38*, 193–224.

Herreshoff, H. C., & Newman, J. N. (1966). The study of sailing yachts. *Scientific American, 215,* August issue, 61–68.

von Karman, T. (1954). *Aerodynamics*. New York: McGraw-Hill.

(A delightful little book, written for the nonspecialist, full of historical anecdotes and at the same time explaining aerodynamics in the easiest way.)

Kuethe, A. M., & Chow, C. Y. (1998). *Foundations of Aerodynamics: Basis of Aerodynamic Design*. New York: Wiley.

Lighthill, M. J. (1986). *An Informal Introduction to Theoretical Fluid Mechanics*. Oxford, England: Clarendon Press.

Liu, T., Kuykendoll, K., Rhew, R., & Jones, S. (2006). Avian Wing Geometry and Kinematics. *AIAA J, 44*, 954–963.

Ramamurti, R., & Sandberg, W. C. (2001). Computational Study of 3-D Flapping Foil Flows. AIAA Paper. 2001–0605.

Supplemental Reading

Ashley, H., & Landahl, M. (1965). *Aerodynamics of Wings and Bodies*. Reading, MA: Addison-Wesley.

Batchelor, G. K. (1967). *An Introduction to Fluid Dynamics*. London: Cambridge University Press.

Karamcheti, K. (1980). *Principles of Ideal-Fluid Aerodynamics*. Melbourne, FL: Krieger Publishing Co.

Millikan, C. B. (1941). *Aerodynamics of the Airplane*. New York: John Wiley & Sons.

Prandtl, L. (1952). *Essentials of Fluid Dynamics*. London: Blackie & Sons Ltd.

(This is the English edition of the original German edition. It is very easy to understand, and much of it is still relevant today. Printed in New York by Hafner Publishing Co. If this is unavailable, see the following reprints in paperback that contain much if not all of this material.)

Prandtl, L., & Tietjens, O. G. (1934). [original publication date]. *Fundamentals of Hydro and Aero-mechanics*. New York: Dover Publ. Co.

Prandtl, L., & Tietjens, O. G. (1934). [original publication date]. *Applied Hydro and Aeromechanics*. New York: Dover Publ. Co.

(This contains many original flow photographs from Prandtl's laboratory.)